Supplementary Information for

The Products of 5-Fluorouridine by the Action of the Pseudouridine Synthase TruB Disfavor One Mechanism and Suggest Another

Edward J. Miracco[1] and Eugene G. Mueller*[,2]

[1]*Department of Chemistry and Biochemistry, University of Delaware, Newark, DE 19716*

[2]*Department of Chemistry, University of Louisville, Louisville, KY 40292*

Skeletal Assignment of the Dinucleotide Products

The full characterization of the products of F^5U from the action of TruB starts with the assignment of all cytidine resonances in the major product, beginning with H^6. For free cytidine at neutral pH, δ_{H^6} = 7.833 ppm and $^3J_{H^5\text{-}H^6}$ = 7.58 Hz, and in the major product, $\delta_{H}6$ = 7.908 ppm and $^3J_{H^5\text{-}H^6}$ = 7.59 Hz. A comparison of the $^3J_{H^5\text{-}H^6}$ values allows the definitive assignment of this resonance as the H^6 proton of the major dinucleotide product 3′-cytidine.

After a specific proton resonance is correctly assigned, the attached carbon can be assigned through the use of the heteronuclear single quantum coherence (HSQC) NMR pulse sequence. Two dimensional HSQC spectra contain proton and carbon chemical shifts on perpendicular axes, with cross peaks correlating carbons to their attached protons.[1,2] Due to the additional resolution obtained by "spreading out" the proton resonances along the carbon dimension, every proton and carbon can be clearly annotated for both the major and minor products (Figure S1). A variant of the HSQC pulse sequence, the heteronuclear multiple bond correlation (HMBC) NMR experiment, correlates attached protons and carbons, two and three bonds away, with 4 bond correlation occasionally observed.[1,2]

Through the use of the HSQC correlation to H^6, C6 is assigned at 143.9 ppm.[†] The carbonyl carbons are then assigned by correlation to H^6 in the HMBC spectrum and are differentiated by chemical shift (C2, 160.3 ppm; C4, 168.8 ppm) (Figure S2). To finalize the nucleobase assignment, it remained to assign H^5. That was achieved using correlated spectroscopy (COSY) to correlate vicinal protons, which show as cross-peaks in the 2D COSY spectrum (Figure S3).[1,2] The correlation to H^6 allows assignment of H^5, (6.083 ppm) and its HSQC correlation reveals C5 at 99.0 ppm. Correlation in the HMBC spectrum to cytidine C6 allows the assignment of $H^{1'}$ (5.972 ppm) (Figure S4), and C1′ (92.2 ppm) is assigned by HSQC correlation. Through COSY correlation to $H^{1'}$, $H^{2'}$ (4.291 ppm) is assigned (Figure S5), which leads to the identification of C2′ (76.7 ppm) by HSQC correlation. The assignment of $H^{3'}$ was achieved using total correlation spectroscopy (TOCSY). Cross-peaks observed in 2D TOCSY spectra correlate protons within the same spin system, and in the case of nucleosides, all ribose protons exist in the same spin system (Figure S6).[1,2] The TOCSY correlation to $H^{1'}$ assigns $H^{3'}$ (4.307 ppm), and the HSQC correlation to $H^{3'}$ reveals the position of C3′ (71.7 ppm). From the TOCSY correlation to $H^{3'}$, $H^{4'}$ (4.238 ppm) is deduced, which establishes C4′ (84.9 ppm) based on correlation in the HSQC spectrum. To finish the assignment of cytidine in the major product, $H^{5'}$/$H^{5''}$ (4.247/4.115 ppm) are assigned by TOCSY correlation to $H^{4'}$ and correlation to phosphorus detected by ^{1}H-^{31}P HSQC (Figure S7); C5′ (66.8 ppm) is assigned by its correlation to $H^{5'}$ and $H^{5''}$, as well as by its sign in the distortionless enhancement by polarization transfer-edited HSQC spectrum (DEPT-HSQC), which detects methylene nuclei as negative peaks and methyl and methyne nuclei as positive peaks.[1,2]

[†]HMBC sometimes detects one bond C–H coupling, and this "breakthrough" appears as a doublet crosspeak with a spacing of $^1J_{CH}$ centered on the correlated proton resonance. This situation applies to C6, with a breakthrough seen at 143.9 ppm correlated to the $\delta_{H}6$ value observed in the 1D proton spectrum and so further confirming the assignment of C6 (Figure S2).

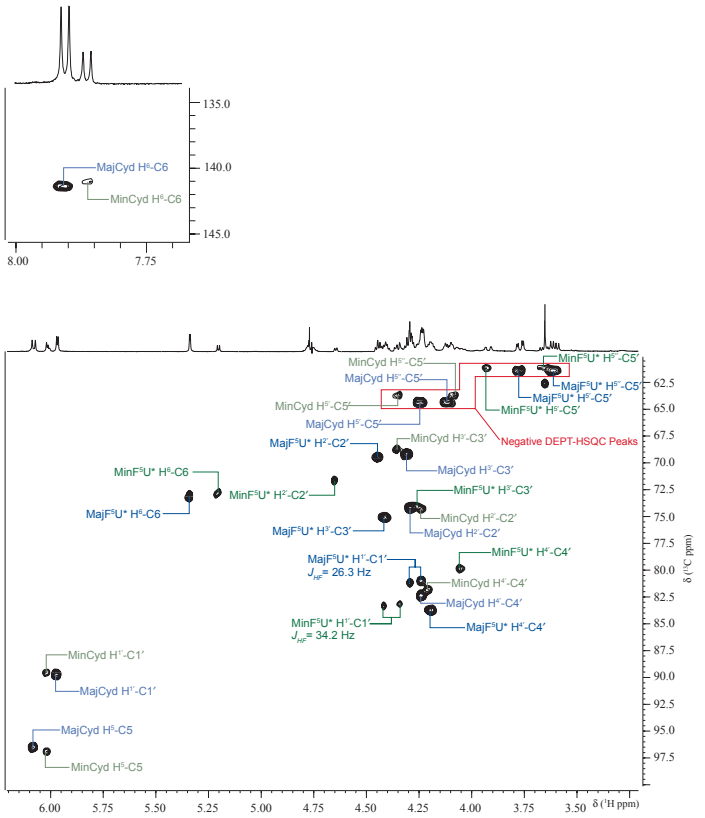

Figure S1. The fully assigned HSQC of the dinucleotide products. (*inset*) The cytidine H^6-C6 correlations. F^5U*, the product of F^5U from the action of TruB; Cyd, cytidine; Maj and Min, the major and minor products, respectively.

During the final isolation of the products, the minor product largely resolved from the major product so that a sample composed of 92% minor product was obtained and analyzed (Figure S8). This fortunate turn of events allowed the minor product cytidine to be assigned in the same manner as the major product cytidine except instead of TOCSY correlations, the pentose protons were sequentially assigned by a COSY walk originating at $H^{1'}$ (Figure S9). The respective carbons were then assigned by HSQC correlations to the assigned pentose protons.

With the complete assignment of the cytidine residues in both dinucleotide products, it remained to assign the other "half" of each dinucleotide—that resulting from the action of TruB on F^5U. For convenience, that moiety will be denoted F^5U*. Assignment of the F^5U* resonances starts with the ^{1}H-^{19}F HSQC spectrum (Figure S10), which shows two protons correlated with each F^5 (major: δ_F = –194.8 ppm, δ_H = 4.264 and 5.340 ppm; minor: δ_F = –175.2 ppm, δ_H = 4.377 and 5.206 ppm). In principle, these F-coupled protons could be either H^6 or $H^{1'}$ in a rearranged product (that is, one with a C1′–C5 glycosidic bond). Because of its clearer TOCSY spectrum, F^5U* of the minor product will be treated first. The proton at 5.206 ppm distinctly lacks correlation to protons in the TOCSY spectrum whereas the other F-coupled proton (4.377 ppm) is correlated to five other protons (Figure S11). This set of correlations can only hold if H^6 lies at 5.206 ppm (in contact with no other protons on the pyrimidine ring) and $H^{1'}$ lies at 4.377 ppm (in contact with the other pentose protons). The assignment of the five protons coupled to $H^{1'}$ proceeds by assigning

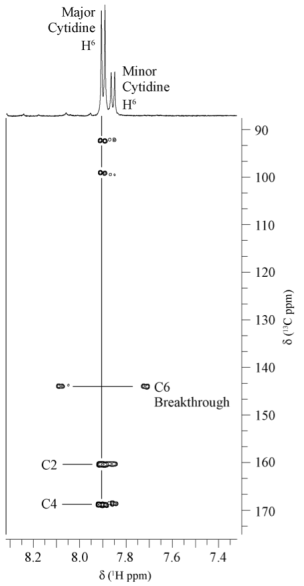

Figure S2. The HMBC spectrum allowing the assignment of C2 and C4 of the major product cytidine.

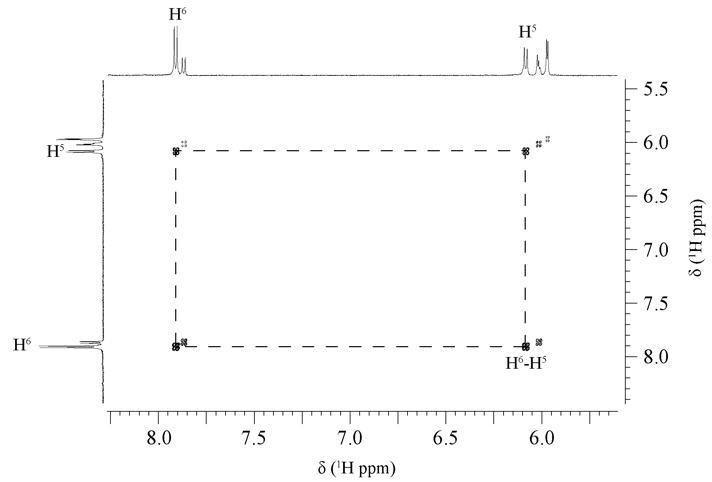

Figure S3. The COSY spectrum of the products allowing the assignment of the major product cytidine nucleobase to be finished by correlating H^6 to H^5.

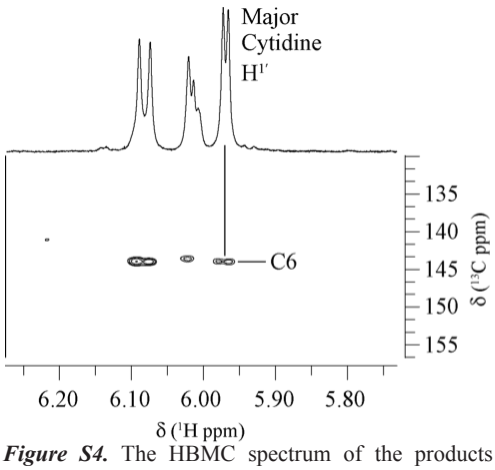

Figure S4. The HBMC spectrum of the products bridging the nucleobase and ribose assignments through correlation of the major cytidine C6 to $H^{1'}$.

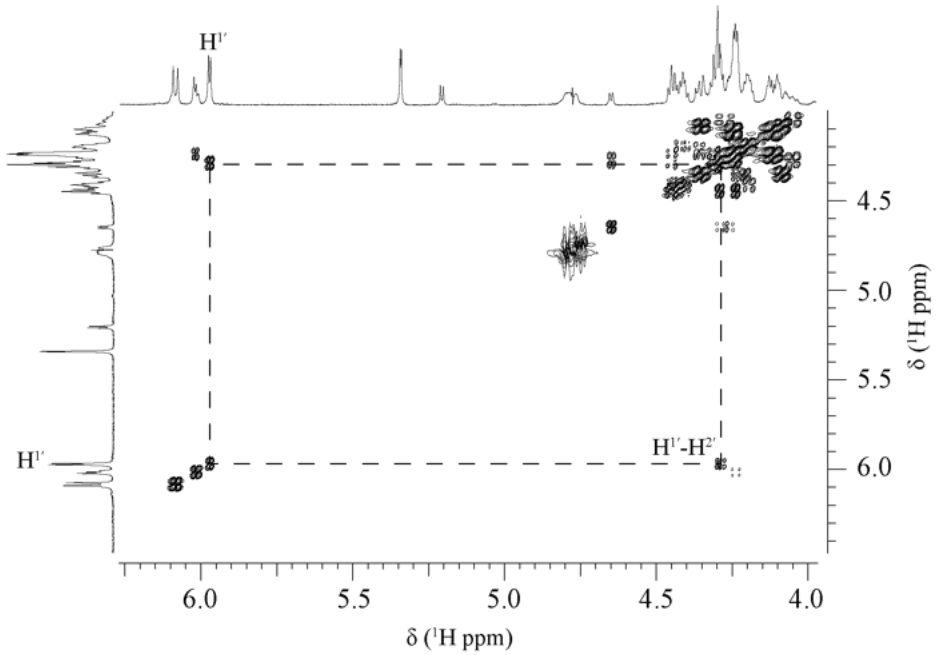

Figure S5. The COSY spectrum of the products allowing the assignment of $H^{2'}$ in the major product cytidine by correlation to $H^{1'}$.

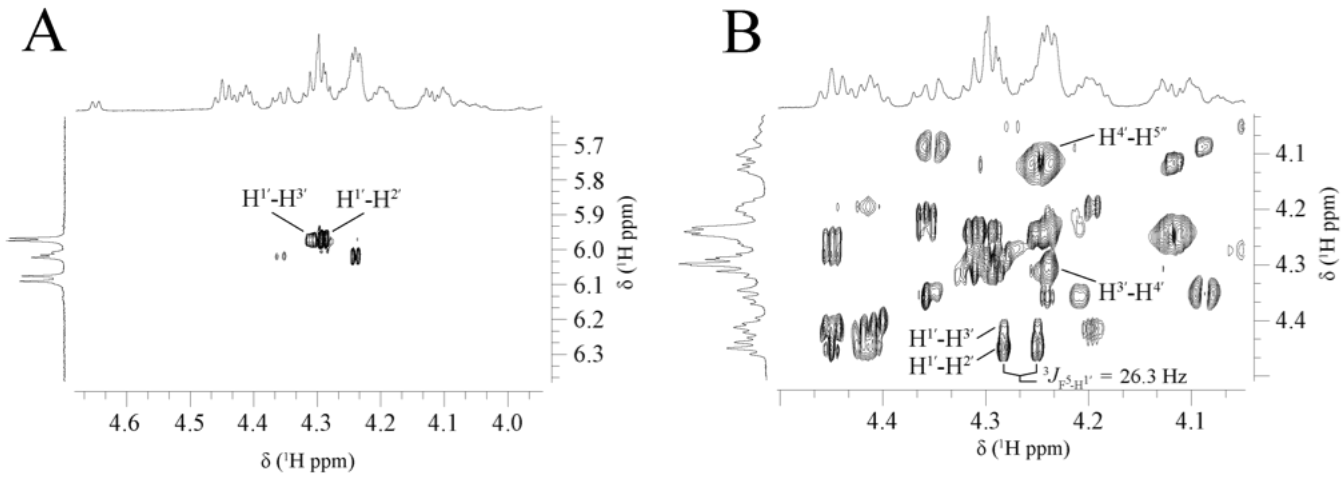

Figure S6. The TOCSY spectrum of the products. (A) The assignment of $H^{2'}$ and $H^{3'}$ in the major cytidine through correlation to $H^{1'}$. (B) The assignment of $H^{4'}$ and $H^{5''}$ in the major product cytidine and the assignment of $H^{2'}$ and $H^{3'}$ in the major product F^5U* by correlation to $H^{1'}$.

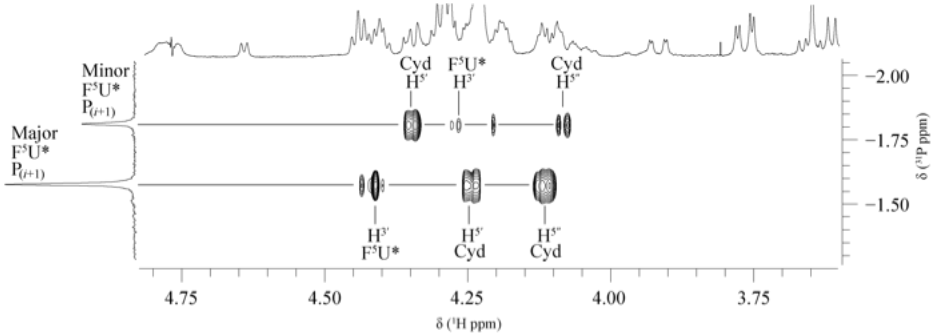

Figure S7. The ^{1}H-^{31}P HSQC spectrum of the products. Correlation between H$^{5'}$ and H$^{5''}$ of cytidine and H$^{3'}$ of both products' F^{5}U* with phosphorus confirms the proton assignments.

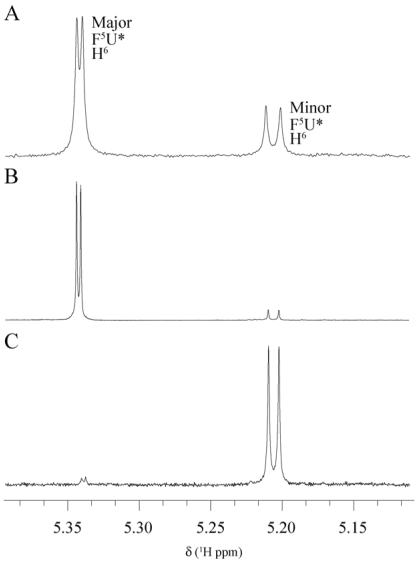

Figure S8. The ^{1}H NMR spectra of fractions from the last purification of products. (A) The products isolated earlier as a mixture. (B) A fraction highly purified in the major product. (C) A fraction highly purified in the minor product.

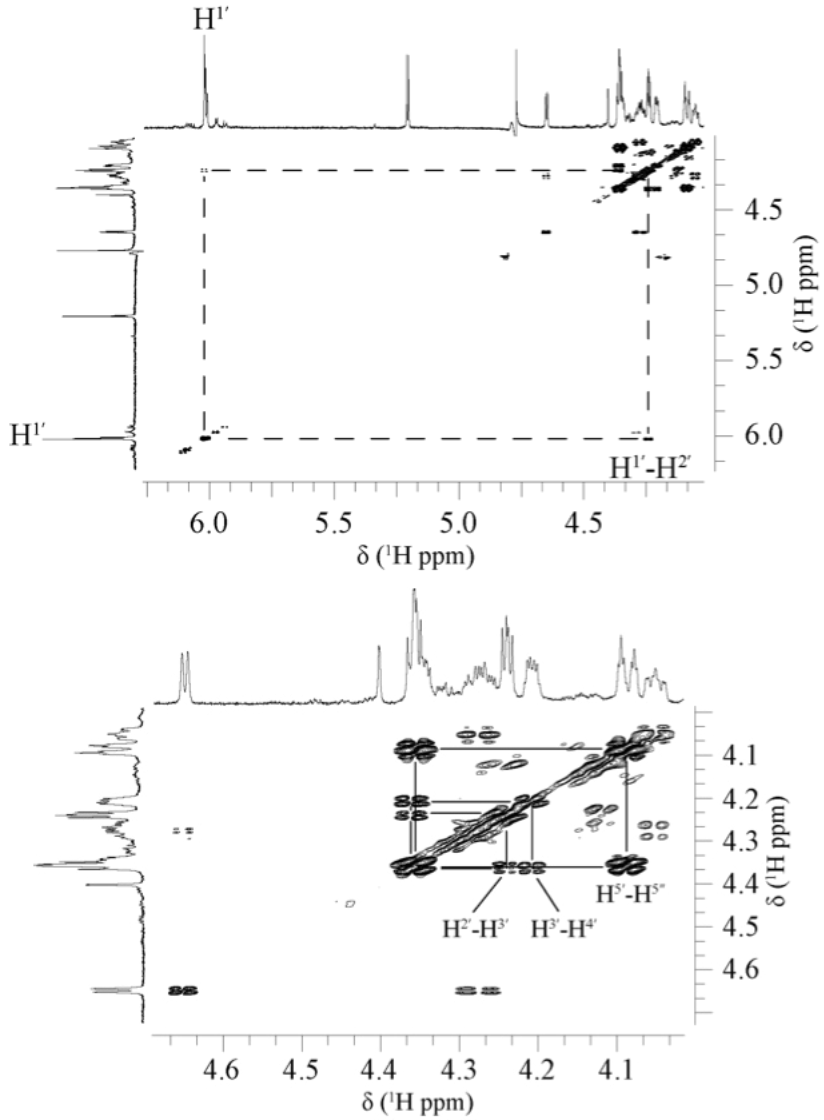

Figure S9. The COSY spectrum of the isolated minor product allowing the complete assignment of its cytidine.

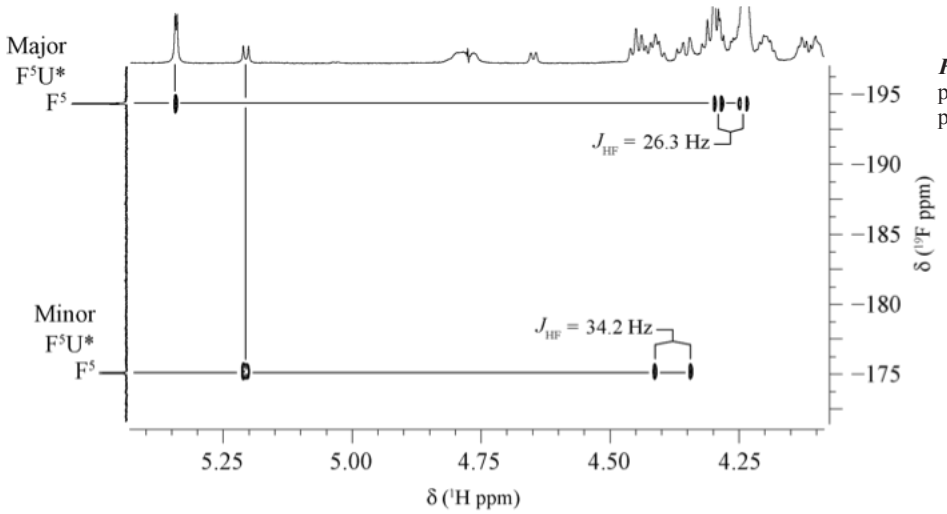

Figure S10. The ^{1}H-^{19}F HSQC spectrum of the products. The two protons correlated with F^5 in both products could be either H^6 or $H^{1'}$.

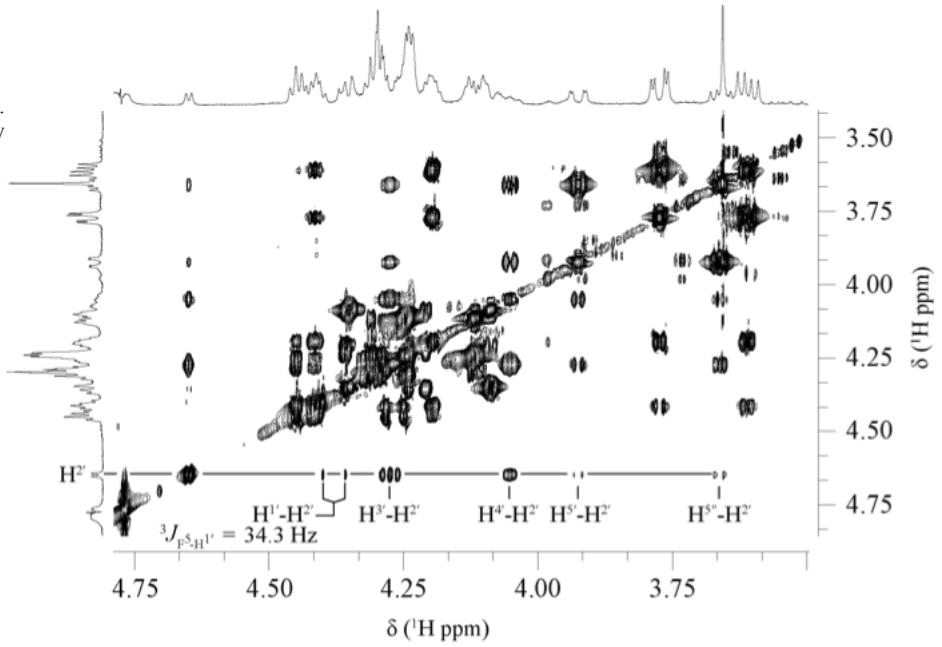

Figure S11. The TOCSY spectrum of the products. The pentose spin system of the minor F^5U^* is clearly observable by correlation to the deshielded $H^{2'}$.

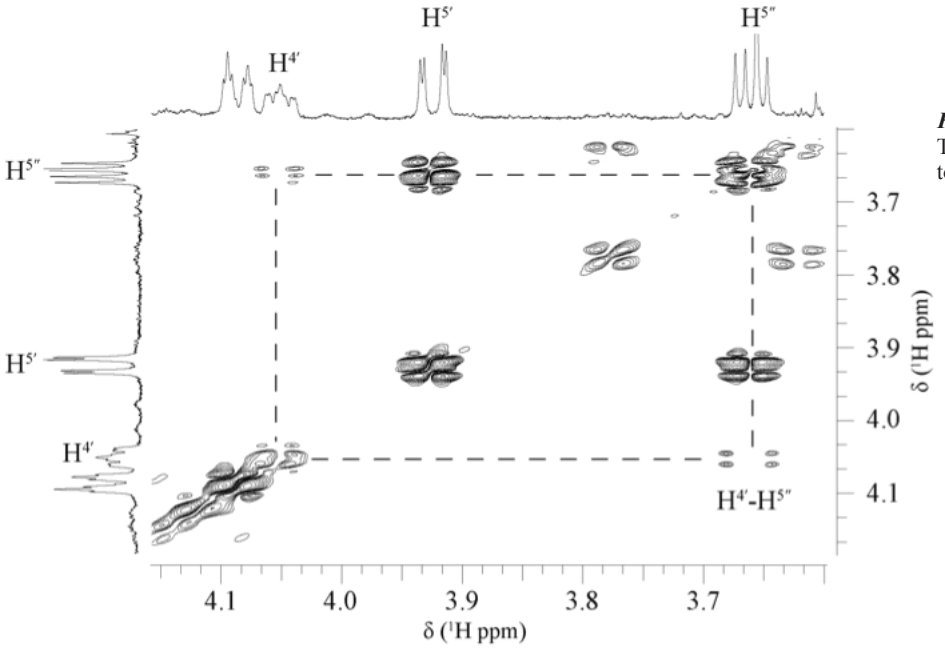

Figure S12. The COSY spectrum of the minor product. The assignment of $H^{4'}$ of F^5U^* is achieved by correlation to $H^{5''}$ in the F^5U^* moiety.

$H^{5'}/H^{5''}$ (3.926/3.661 ppm) by their sign in the DEPT-HSQC spectrum. From $H^{5'}/H^{5''}$, $H^{4'}$ (4.051 ppm) is assigned by COSY correlation (Figure S12). To differentiate between the remaining two sugar protons, $H^{3'}$ (4.278 ppm) is identified by coupling to phosphorus in the ^{1}H-^{31}P HSQC spectrum (Figure S7), and $H^{2'}$ (4.649 ppm) is assigned by elimination. The identities of the pentose carbons are each established by HSQC correlation to their attached protons. Moving on to the nucleobase of F^5U*, H^6 is correlated to two carbonyl carbons in the HMBC spectrum, C2 (155.7 ppm) and C4 (168.4 ppm) (Figure S13), which are assigned on the basis of their relative chemical shifts.

The deshielded $H^{2'}$ of F^5U* in the minor product allowed an unobstructed view of the entire pentose spin system by TOCSY correlation; unfortunately, $H^{2'}$ of F^5U* in the major product is more shielded, so overlap with other cross-peaks muddle assignment of its TOCSY correlations. Therefore, the assignment begins with $H^{5'}/H^{5''}$ (3.774/3.609 ppm), which are assigned from their sign in the DEPT-HSQC spectrum because they are the fourth and final set of diastereotopic protons observed. COSY (Figure S14) correlation then allows the assignment of $H^{4'}$ (4.194 ppm), and analysis of the ^{1}H-^{31}P HSQC allows unambiguous assignment of $H^{3'}$ (4.413 ppm). The ^{1}H-^{19}F HSQC allows assignment of $H^{1'}$ (4.264 ppm) and H^6 (5.340 ppm), which are differentiated by TOCSY correlation of $H^{1'}$ to two other protons: $H^{2'}$ (4.449 ppm) and $H^{3'}$. The ribose carbons are assigned by HSQC correlation to their respective protons, and carbonyl resonances of the F^5U* nucleobase by HMBC correlation to H^6.

The F^5U Products are C-Glycoside Isomers of Hydrated F^5U. The determination of both F^5U* skeletal structures unambiguously demonstrates that *both* the major and minor products have been rearranged to *C*-glycosides. In support of this key assignment, the expected magnitude for vicinal coupling between F^5 and $H^{1'}$ and HMBC correlations between $H^{2'}$ and C5 are both observed.[3]

A well documented phenomenon among fluorinated nucleosides are long range J_{HF}, saliently the $^{5}J_{F^5\text{-}H^{1'}}$ of F^5U when the nucleobase is *anti* to the ribose.[4,5] With this in mind, care must be taken to ensure the observed couplings between F^5 and $H^{1'}$ in both F^5U* are in fact vicinal and not long range. The magnitude of couplings are the primary method for differentiating vicinal and long range couplings.[1,2] In both products, the couplings are quite large: $J_{F^5\text{-}H^{1'}} = 26.3$ Hz in the major product and 34.2 Hz in the minor product (Figure S15). Long range couplings are typically much smaller (in F^5U, for example,

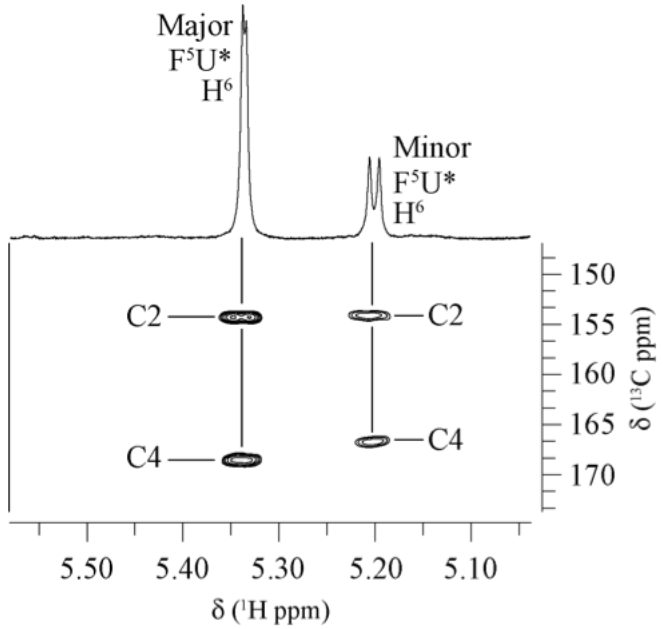

Figure S13. The HMBC spectrum of the products. The assignment of the major and minor F^5U* carbonyl resonances are achieved through correlation to their respective H^6 protons.

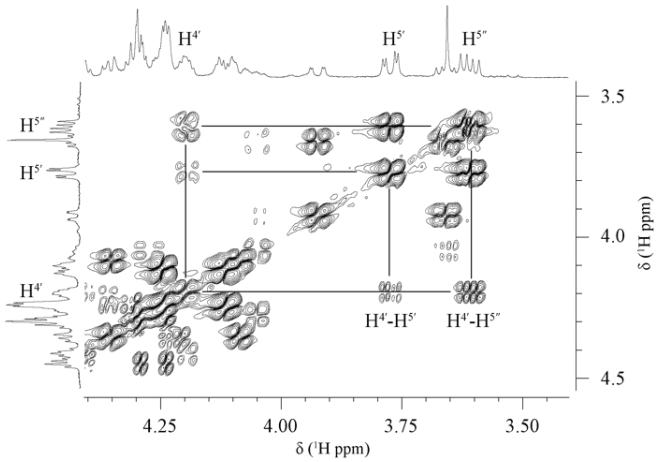

Figure S14. The COSY spectrum of the products. The assignment of $H^{4'}$ of F^5U* in the major product is achieved by its correlation to $H^{5'}$ and $H^{5''}$.

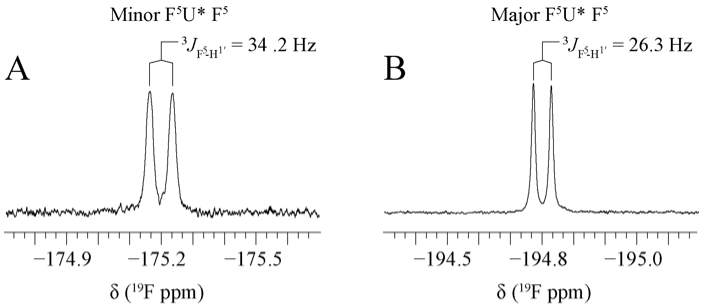

Figure S15. The ^{19}F NMR spectrum of the products. (A) The region containing the minor product F^5. (B) The region containing the major product F^5. The magnitude of the $^{3}J_{HF}$ observed supports a vicinal relationship between F^5 and $H^{1'}$ in both the major and minor products.

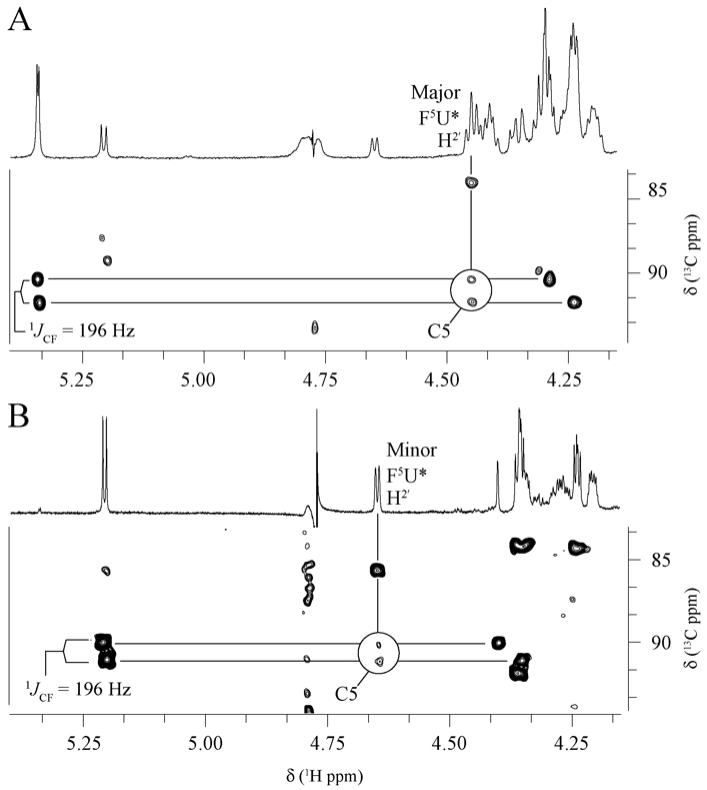

Figure S16. The HMBC spectra of the products. (A) The mixture of both products. (B) The isolated minor product. Both spectra display the correlation observed between $H^{2'}$ and C5, an observation that could only occur if both products were rearranged *C*-glycosides.

$^5J_{F^5\text{-}H^{1'}}$ = 1.8 Hz), so the large couplings in both products indicate a vicinal relationship between F^5 and $H^{1'}$. The HMBC spectra further support the assignment of vicinal $H^{1'}$ and F^5 in both of the products and, by extension, their rearrangement to *C*-glycosides. In a *C*-glycoside, $H^{2'}$ and C5 are separated by three bonds, a distance that affords detection by HMBC, whereas in an *N*-glycoside, $H^{2'}$ and C5 are separated by five bonds, which is beyond the detection limit of HMBC.[1] Upon inspection, $H^{2'}$ and C5 correlations are clearly observed (Figure S16) in the HMBC spectra of both products. Additionally, the distinct lack of any correlations to C5 in the HSQC spectra as well as the large $^1J_{CF}$ observed for C5 in the HMBC spectra (Figure S16), support a fluorinated C5 that does not have an attached proton, further confirming that both TruB products are rearranged *C*-glycoside isomers of F^5U.

Identification of the Two Products of F^5U from the Action of TruB

The next step in the structural elucidation was to determine the difference in the major and minor products, which could be due to either structural or conformational isomerism. To investigate the latter, NMR spectra were acquired at variable temperature and field, and the trailing cytidine was chemically degraded. To investigate stereoisomerism, spatially sensitive NMR experiments (homo- and heteronuclear Overhauser spectroscopy and residual dipolar coupling methods) were utilized in conjunction with *in silico* analysis.

Examination of Conformational Isomerism

Variable Temperature and Field. The average lifetime equivalent resonances remain in each conformation is quantified by the exchange time (τ_{ex}). The relationship between τ_{ex} and the correlation time (τ_c), colloquially known as the 'NMR time scale', determines the spectral appearance of the exchanging resonances.[1,2,6] When $\tau_c << \tau_{ex}$, the two exchanging peaks are well resolved, and the two conformations are said to be in slow exchange. When τ_c approaches τ_{ex} (intermediate exchange), the two peaks broaden and begin moving toward one another. When $\tau_c >> \tau_{ex}$, fast exchange applies, and the peaks coalesce into a single, sharp peak between the two original peaks. To determine if a pair of resonances are related by conformational exchange, τ_{ex} can be altered by acquiring spectra at varying temperatures, or τ_c can be altered by acquiring spectra at different magnetic field strengths ($\mathbf{B_0}$). A decreasing $\mathbf{B_0}$ decreases τ_c, so decreasing $\mathbf{B_0}$ leads to the same spectral effect as increasing the acquisition temperature.[1,2,6]

Variable temperature ^{1}H NMR (6 °C, 20 °C and 25 °C) was run with the NMR sample containing a mixture of both the major and minor products. The chemical shifts, line widths, *J*-couplings, and integration values of H^6 in both products did not change beyond the error in measurement; the same results were also observed for H^6 in the cytidine residue of both products. Additionally, no changes were observed when spectra were recorded at 400, 500, 600, 700, and 800 MHz. In the later samples of largely separated major and minor products, the other product did not noticeably grow in over months, even after multiple rounds of drying *in vacuo* at 30 °C, 45 °C, and 60 °C, snap freezing in liquid nitrogen, storage at –80 °C, and thawing. These results all argue that the major and minor products are not simply different conformers.

In further support of this position, the ratio of the two products when isolated together was never perturbed from the integration ratio in the ^{19}F NMR spectra acquired immediately after reaction, even with passage through both aqueous and non-polar media, multiple rounds of heating to 100 °C, freezing in liquid nitrogen, storage at –80 °C and on ice, digestion to dinucleotides, subsequent HPLC purification, and multiple dryings *in vacuo*. If the major and minor products are simply conformers, they exist in an astonishingly strongly locked conformation, independent of whether the F^5U* is part of an oligo- or a di- nucleotide.

In an attempt to see if a locked conformation was the cause of the divergent HPLC retention times and NMR spectra, the 3′-cytidine of both dinucleotide products was removed. Due to the flexibility of the phosphodiester bond, it is possible that cytidine resides in two different positions relative to F^5U during product formation. After release of the non-canonical product, equilibration between the states could be restricted, leaving two distinct products. An ancillary reason for removing the trailing cytidine was to simplify the NMR spectrum. Periodate degradation was chosen over enzymatic digestion to limit the addition of buffer species that would contaminate the NMR spectra and because trial enzymatic digestions with purchased dinucleotides resulted in only partial digestion within a reasonable time frame.

A sample containing both the major and minor products was incubated with 10-fold excess periodate under basic conditions, acidified, and then neutralized.[7,8] The F^5U*-3′-phosphate was purified using a bed of weak anion exchanging media in a Pasteur pipette and eluted by a step-wise gradient of ammonium carbonate, pH 8. The product had an NMR spectrum that closely matched F^5U* of the major dinucleotide product (Figure S17, Table S1); the yield was approximately 40% of the total products in the initial sample as judged by comparison of the integration of H^6 to that of 4,4-dimethyl-4-silapentane-1-sulfonate-d_6 (DSS), the internal chemical shift reference. No product with a spectrum similar to the modified F^5U in the minor dinucleotide product was detected.

Selective loss of the minor product may arise from the removal of the component that locks two differing conformations so that initial minor product converts to major product after degradation. If loss of the minor product were proportional to that of the major product, however, the concentration of the minor product would drop to the very threshold of NMR detection. Alternatively, the minor product

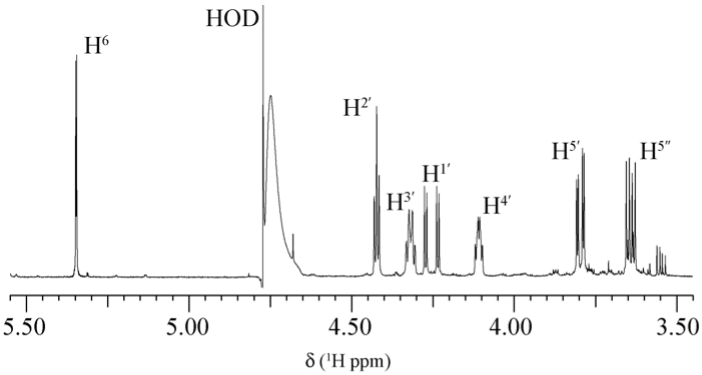

Figure S17. The ^{1}H spectrum of isolated F^5U* 3′-phosphate, which bears a striking resemblance to the major product.

Table S1. Chemical shifts (ppm) for F^5U* in the major product dinucleotide (F^5U*pC) and in isolated F^5U* 3′-phosphate

	F^5U*pC	F^5U* 3′-P	Δδ
H^6	5.340	5.346	– 0.006
$H^{1'}$	4.264	4.253	0.011
$H^{2'}$	4.449	4.423	0.026
$H^{3'}$	4.413	4.318	0.095
$H^{4'}$	4.194	4.109	0.085
$H^{5'}$	3.774	3.796	0.022
$H^{5''}$	3.609	3.641	– 0.032
C6	75.7	75.6	0.100
C1′	83.6	84.2	– 0.600
C2′	72.0	72.6	– 0.600
C3′	77.6	76.3	1.300
C4′	86.2	86.1	0.100
C5′	63.9	64.3	– 0.400

may be more sensitive to the degradation conditions. Without a yield greater than the original amount of major product dinucleotide, the selective loss of the minor product cannot be definitively interpreted. Although the periodate results may be construed to suggest conformational isomerism, the variable temperature and $\mathbf{B_0}$ experiments and the tenacity of the major and minor products in retaining their initial ratio through dramatic environmental changes support stereochemical isomerism over conformational isomerism.

Examination of Stereochemical Isomerism

Testing for Stereochemical Differences at C5 and C6. After the initial discovery that TruB was capable of turning over [F^{5}U]TSL into two distinct products[9], preliminary NMR experiments by Spedaliere and Mueller on the products suggested stereo-random hydration at C6 after release of rearranged F^{5}U, with a single stereo configuration at C5 (*S*) as seen in the cocrystal of TruB and [F^{5}U]TSL.[10] Spedaliere and Mueller hypothesized that the major product has the stereochemistry seen in the cocrystal structure[10]—5*S*,6*R*—and so the stereochemistry of the minor product was 5*S*,6*S* (Figure S18, **1** and **2**). This hypothesis was a reasonable starting point, but in the interest of completeness, the candidate list was expanded to include the possibility that the products differed in configuration at C5 as well—5*R*,6*S* and 5*R*,6*R* (Figure S18, **3** and **4**). One must also consider that each stereoisomer can differ in its glycosidic rotational conformation (described by the angle χ), resulting in four additional candidate structures (Figure S18, **5**-**8**). All eight structures were subjected to density functional theory (DFT) energy minimization by geometrical optimization. After convergence, H^6-H^{ribose} and F^5-H^{ribose} distances were measured (Table S2).

The first step in excluding candidate structures was to determine the relative location of F^5 in both products. The *J*-coupling values of F^5 and H$^{1'}$ are exceptionally large; $^3J_{H^{1'}\text{-}F^5}$ is 26.3 Hz in the major and 34.2 Hz in the minor product, which limit the dihedral angle (ϕ) between F^5 and H$^{1'}$ to ~180° or ~0°. In a *cis* orientation (ϕ = 0°), F^5 and H$^{1'}$ are much closer spatially than if they exist in a *trans* orientation (ϕ = 180°), a difference detectable by one dimensional ^{1}H-^{19}F heteronuclear Overhauser effect spectroscopy, "HOESY". The integration values of H$^{1'}$, H$^{2'}$, and H$^{3'}$ are sensitive to their relative distance from F^5 and are, therefore, good probes to determine the conformation about the glycosidic bond. If F^5 resides *cis* to H$^{1'}$, the expected spectral appearance would be a larger integration of H$^{1'}$ compared to H$^{2'}$ and H$^{3'}$; whereas if F^5 is *trans* to H$^{1'}$, the integrations of H$^{2'}$ and H$^{3'}$ would be larger than H$^{1'}$. The H$^{1'}$ integration values in *both* products are considerably smaller than the integration values of H$^{2'}$ and H$^{3'}$ (Figure S19, Table S3). This proves the major and minor products exist with a dihedral angle between F^5 and H$^{1'}$ near 180°, a *trans* relationship, which leaves only four possible structures (**1**-**4**).

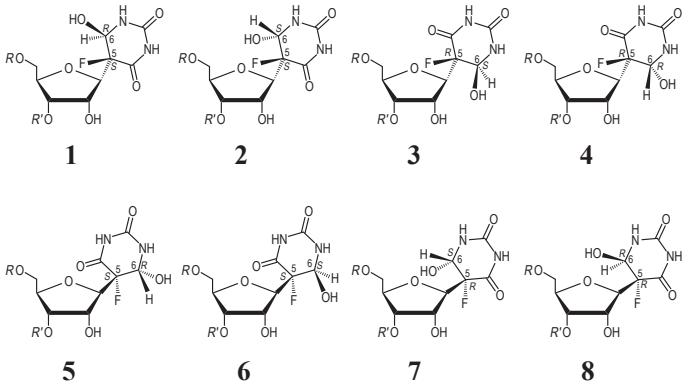

Figure S18. Candidate structures for the products. **1**, the structure observed in the cocrystal structure and the proposed major product; **2**, the proposed minor product with inverted stereochemistry at C6. The two additional permutations of stereochemistry at C5 and C6—5*R*,6*S* (**3**) and 5*R*,6*R* (**4**), and glycosidic rotamers of the four candidate stereoisomers (**5**-**8**).

To differentiate between these four structures, key differences in the proximity of H^6 to H$^{2'}$ and H$^{1'}$ should be observable in the NOESY spectrum. In the DFT optimized 5*R*,6*S* and 5*R*,6*R* isomers, the H^6-H$^{2'}$ and H^6-H$^{1'}$ distances are similar (Table S2), suggesting that the NOE intensity observed between H^6 and both H$^{2'}$ and H$^{1'}$ should be similar, which is clearly not true. This leaves two of the initial candidate structures: the stereoisomer seen in the cocrystal structure (5*S*,6*R*), and the minor product originally proposed by Spedaliere and Mueller (5*S*,6*S*) (Figure S18, **1** and **2**). The large amount of NMR data was further scrutinized to seek support for this tentative assignment.

The Deshielded H$^{2'}$. During the skeletal assignment of the minor product it was noted that H$^{2'}$ is dramatically deshielded compared to H$^{2'}$ in the major product. Additionally, specific cross-peaks seen in the major product NOESY—H$^{2'}$-H^6, H$^{2'}$-H$^{5'}$, and H$^{2'}$-H$^{5''}$—are absent in the minor product NOESY (Figure S20 and Figure S21). In an attempt to rationalize these disparate NOE correlations, the distances between these protons obtained from the DFT-optimized structures in the proposed major (5*S*,6*R*) and minor (5*S*,6*S*) products were compared (Table S2, **1** and **2**). The distance between H$^{2'}$ and H^6 in the 5*S*,6*R* and the 5*S*,6*S* isomers are 4.355 Å and 4.723 Å, respectively. This small difference (0.36 Å) suggests that the minor product should

Table S2. Distances (Å) measured in the DFT-optimized structures.

		H$^{1'}$	H$^{2'}$	H$^{3'}$	H$^{4'}$	H$^{5'}$	H$^{5''}$
(**1**) 5*S*,6*R*	F^5	3.314	2.506	4.607	4.647	3.084	4.727
	H^6	3.001	4.355	5.640	4.278	4.340	5.477
(**2**) 5*S*,6*S*	F^5	3.317	2.467	4.568	4.655	2.970	4.638
	H^6	3.835	4.723	6.611	5.906	5.125	6.629
(**3**) 5*R*,6*S*	F^5	3.312	2.495	4.665	4.839	3.622	5.176
	H^6	2.864	3.050	4.961	5.639	5.409	6.517
(**4**) 5*R*,6*R*	F^5	3.313	2.495	4.708	4.827	3.531	5.111
	H^6	3.763	4.262	6.424	6.506	5.952	6.624
(**5**) 5*S*,6*R*	F^5	2.351	3.653	5.394	5.236	5.603	6.624
	H^6	3.644	2.170	4.551	5.395	4.260	5.693
(**6**) 5*S*,6*S*	F^5	2.415	3.521	5.336	5.317	5.471	6.564
	H^6	4.199	3.925	6.208	6.237	5.283	6.833
(**7**) 5*R*,6*S*	F^5	2.722	2.922	5.030	5.402	4.969	6.236
	H^6	2.312	4.620	5.991	5.038	5.817	6.737
(**8**) 5*R*,6*R*	F^5	2.403	3.498	5.349	5.358	5.369	6.522
	H^6	3.528	4.967	6.696	5.795	5.871	7.103

Table S3. HOESY integrations of the major and minor products.

	major	minor
H^6	[1.00]	[1.00]
H$^{1'}$	0.33	0.18
H$^{2'}$	1.00	0.67
H$^{3'}$	0.72	0.85
Cyd H^5	—	0.23

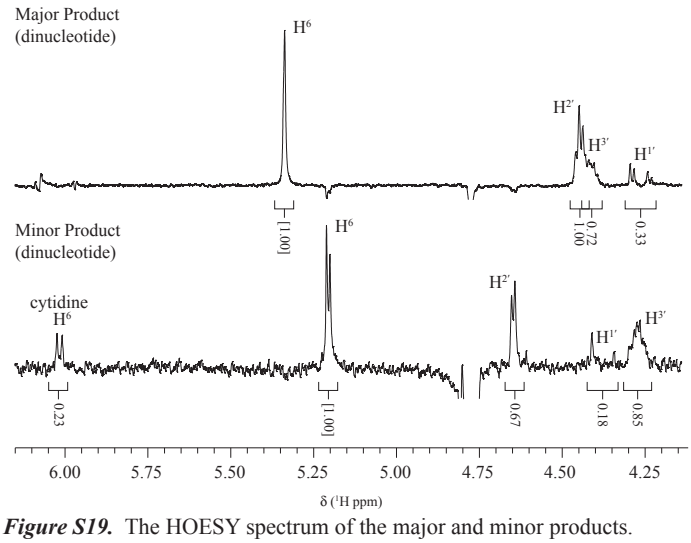

Figure S19. The HOESY spectrum of the major and minor products.

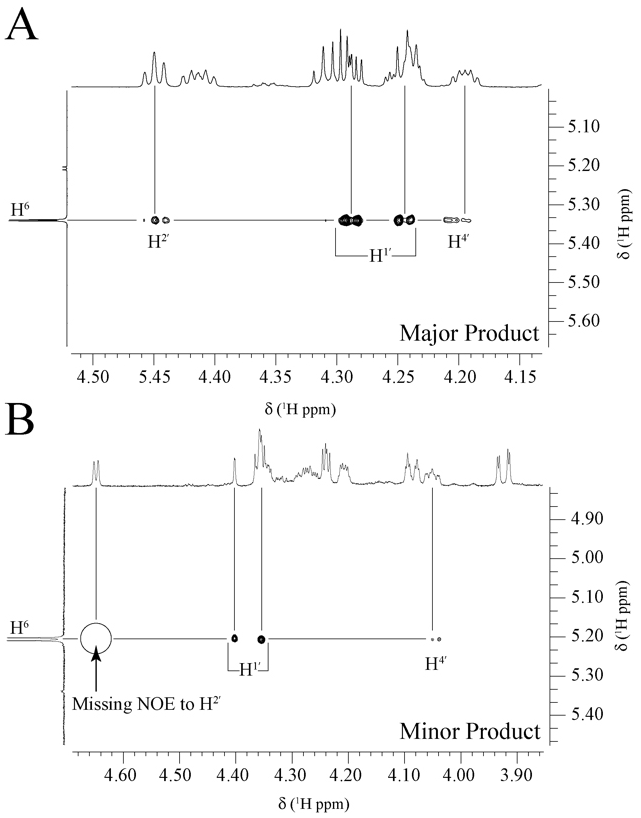

Figure S20. NOESY spectra displaying correlations to H^6 of F^5U* in the (A) major and (B) minor products. Note the larger intensity of $H^{1'}$ compared to $H^{2'}$ in the major product and the distinct absence of correlation to $H^{2'}$ in the minor product.

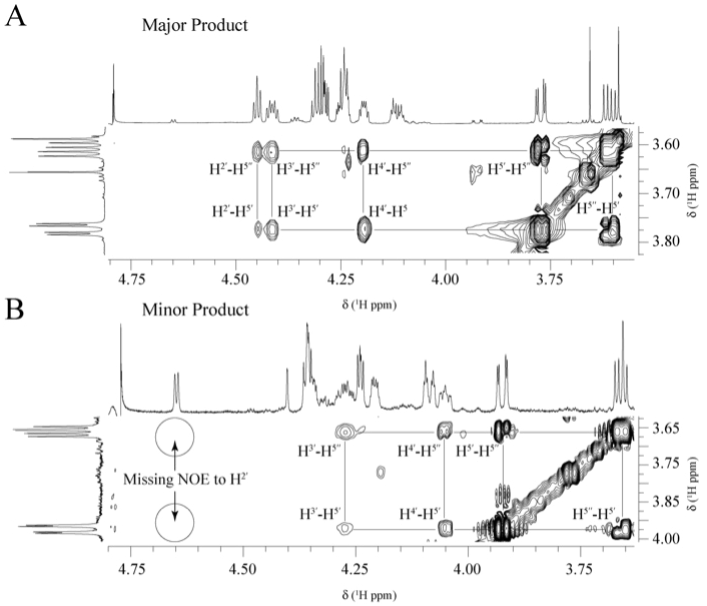

Figure S21. The NOESY spectra of the (A) major and (B) minor products. Note the absence of $H^{2'}$ correlation to both $H^{5'}$ and $H^{5''}$ in the minor product.

display a similar NOE to the major product, which is not observed (Figure S20) and so offers a clue into the difference between the two products: either H^6 or $H^{2'}$ is displaced in the minor product compared to the major product.

The lack of NOESY correlations between $H^{2'}$ and either $H^{5'}$ and $H^{5''}$ (Figure S21) offers an additional clue. The measured distances between $H^{2'}$ and $H^{5'}$ are 2.51 Å in the 5*S*,6*R* isomer and 2.47 Å in the 5*S*,6*S* isomer, a difference of only 0.03 Å. A similarly small difference (0.02 Å) is measured between $H^{2'}$ and $H^{5''}$. These miniscule differences would *not* lead to observed NOE correlations in the major not the minor product. Furthermore, when the O5′-C5′-C4′-$H^{4'}$ dihedral angle (γ) in the 5*S*,6*S* isomer is manually varied *in silico*, the maximal distance between $H^{2'}$ and both $H^{5'}$ protons (with O5′ *trans* to $H^{4'}$), is 3.78 Å, a value inconsistent with the NOE results (Figure S22). Together, these data suggest that the location of $H^{2'}$ and *not* H^6 varies between the two products.

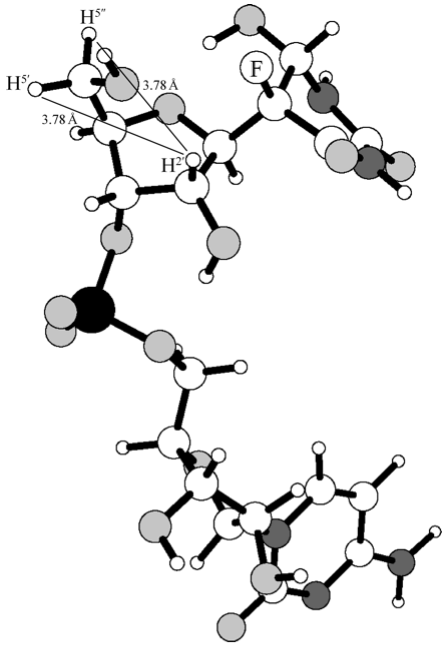

Figure S22. Ball and stick representation of the converged 5*S*,6*S* isomer (**2**, Figure 18) with an O5′-C5′-C4′-$H^{4'}$ dihedral angle that maximizes the distance between $H^{2'}$ and both $H^{5'}$ and $H^{5''}$.

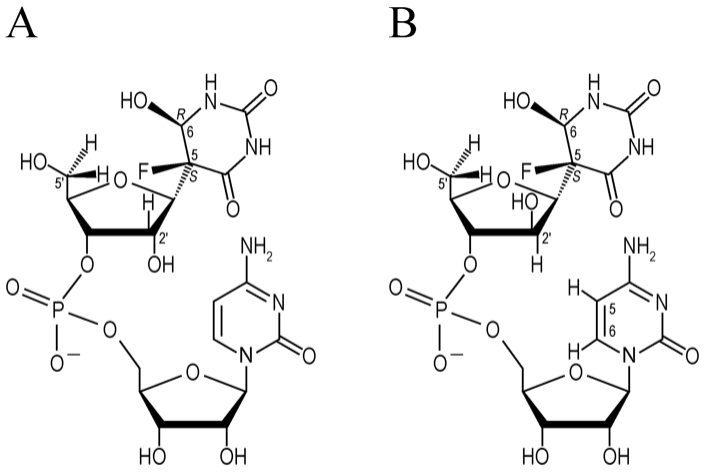

Figure S23. The proposed major (A) and minor (B) products, which are distinguished by epimerization at C2′.

If the location of $H^{2'}$ differs between the products, the HOESY spectra should offer insight due to the central location of F^5. This difference would present as a divergence in the integration ratio observed between $H^{2'}$ and $H^{3'}$ in both products. Based on the optimized 5*S*,6*R* and 5*S*,6*S* isomers, the differences between the two isomers for $F^5\cdots H^{2'}$ and $F^5\cdots H^{3'}$ distances are negligible (0.04 Å for both), so no difference in ratio is predicted. The integration values observed in the major product HOESY spectrum agrees with the prediction, but for the minor product, the integration of $H^{3'}$ appreciably exceeds that of $H^{2'}$ (Table S3). This result clearly agrees with the NOESY data presented earlier, highly suggesting that the minor product is the C2′ epimer, β-D-arabinofuranoside, of the major β-D-ribofuranoside product (Figure S23).

This assignment immediately leads to an additional prediction: if the minor product is an arabinofuranoside, $H^{2'}$ (better denoted as $H^{2''}$ to distinguish the *arabino* C2′) should be pointing "downward" instead of "upward" in a standard Haworth projection, which could

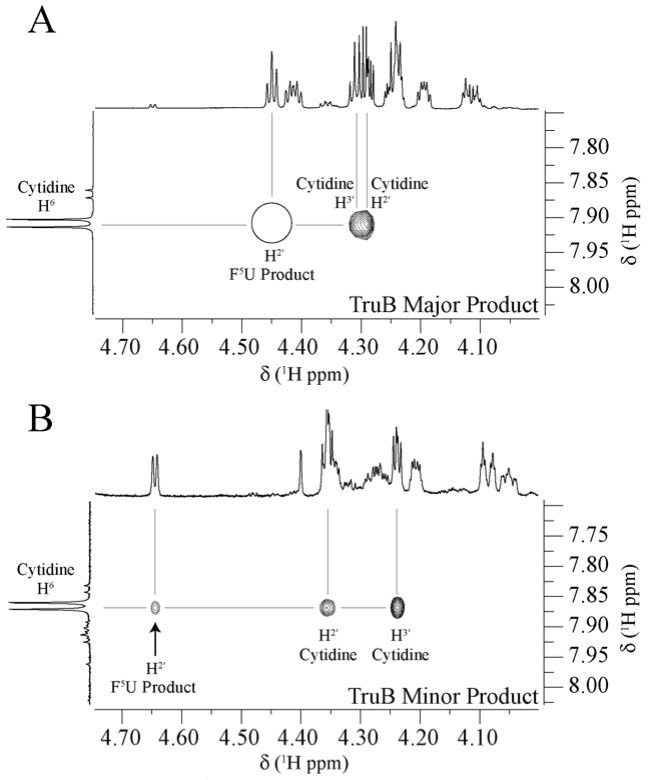

Figure S24. The F⁵U* H⁶ region of the NOESY spectra of the (A) major and (B) minor products. An internucleotide correlation between cytidine H⁶ and F⁵U* H²″ is observed in the minor but not the major product.

result in an internucleotide NOE with cytidine. Such an NOE is clearly observed between cytidine H⁶ and H²″ of F⁵U* in the minor product, with no cognate observed in the major product (Figure S24). The strongest support of an *arabino* minor product comes from the direction of chemical shift changes (Δδ) between the ribose protons of the major and minor products. When these chemical shifts are compared to those of authentic uracil-1-β-D-arabinofuranoside (AraU) and uridine (U), the direction of the Δδ for each pentose proton in the major and minor products matches those seen between uridine and AraU (Figure S25), including the relative direction of the deshielded H²″. This trend appears to be exclusive to arabinonucleosides[11,12], and strongly supports epimerization at C2′ rather than inversion at C6 as the difference between the products.

Residual Dipolar Coupling NMR. To confirm the assignment of the minor product as the C2′ epimer of the major product, residual dipolar coupling (RDC) NMR was carried out on both products. RDC NMR is a rapidly growing technique in small molecule structural elucidation and a less-utilized sibling of dipolar coupling, a widely used method of structure elucidation in solid state NMR.[13-16] The difference between the two is the degree of anisotropy imparted on the molecule of interest by the matrix and thus the magnitude of the dipolar couplings. In RDC NMR, a slightly aligning medium forces the solute molecules to occupy a certain common orientation relative to $\mathbf{B}_0$ for a small period of time relative to the time they tumble freely. Whereas molecules in a homogenous solution tumble equally through all possible alignments with respect to $\mathbf{B}_0$ during acquisition and thus experience net cancellation of the dipolar couplings, the partial alignment causes the molecules to inhabit a common anisotropic state for a small but significant amount of time, preventing the dipolar couplings from completely averaging to zero and thereby leaving small residual ones. These RDCs contain information about the

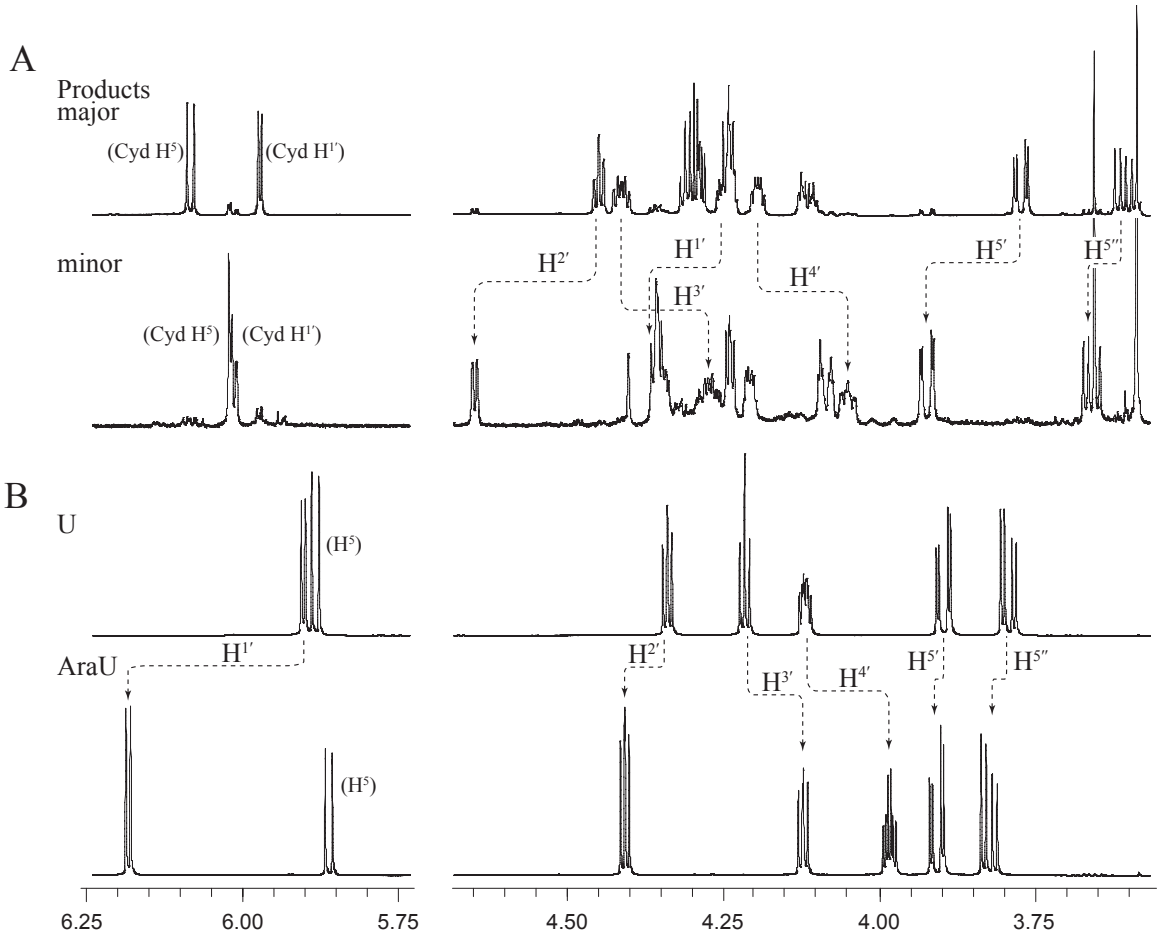

Figure S25. A comparison of chemical shift changes supporting epimerization at C2′ as the difference between the major and minor products. The variation in pentose proton chemical shifts in the major and minor products (A) matches that between uridine and arabinouridine (B).

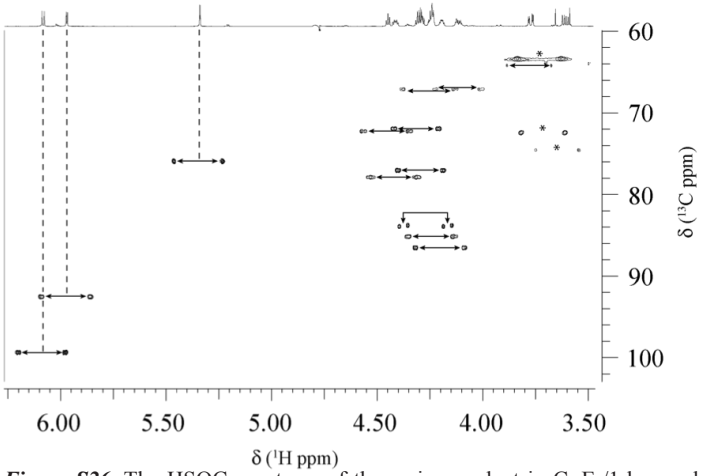

Figure S26. The HSQC spectrum of the major product in $C_{12}E_5$/1-hexanol acquired without ^{13}C-decoupling.

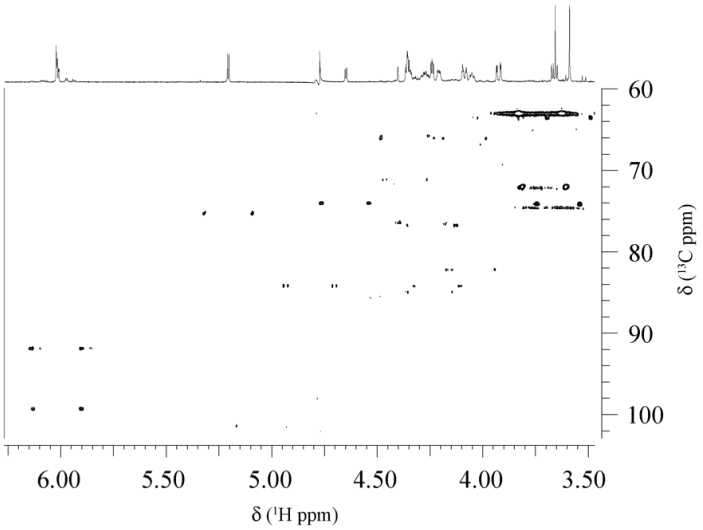

Figure S27. The HSQC spectrum of the minor product in $C_{12}E_5$/1-hexanol acquired without ^{13}C-decoupling.

orientation of bond vectors within a molecule with respect to $\mathbf{B_0}$ and thereby allow the determination of the relative orientation of bonds within a molecule.[17]

The residual dipolar coupling of a proton bonded to a carbon (D_{CH}) is obtained by measuring the total coupling constant (T) between the bonded proton and carbon when the sample is dissolved in an anisotropic medium. Total coupling is related to J and D through Equation S1.

$$|T| = |J + 2D| \tag{S1}$$

The D_{CH} values are then obtained from the coupling values measured in isotropic medium, which is dominated by J-coupling, through rearrangement of Equation S1 to obtain Equation S2.

$$D_{CH} = \frac{T_{CH} - D_{CH}}{2} \tag{S2}$$

The molecular angular position relative to $\mathbf{B_0}$ is determined quantitatively if at least five unique RDC values are observed—allowing solution of the alignment tensor, which is then utilized to calculate the expected RDC values for candidate structures. The experimental and calculated RDC values are compared to arrive at the quality factor (Q) through the use of Equation S3: the lower the Q-factor, the higher the confidence that the candidate structure is the true one.[18]

$$Q = \sqrt{\frac{\sum (D_{exp} - D_{calc})^2}{\sum D^2_{exp}}} \tag{S3}$$

Table S4. Isotropic and anisotropic T-couplings (Hz) obtained from the ^{13}C-coupled HSQC spectra of the major and minor products.

nuclei	isotropic	anisotropic	D_{CH}
Major Product F^{5}U*			
H^6-C6	169.7	159.4	-5.15
H$^{1'}$-C1′	150.9	145.7	-2.60
H$^{2'}$-C2′	152.6	150.9	-0.85
H$^{3'}$-C3′	156.4	156.0	-0.20
H$^{4'}$-C4′	151.3	162.9	5.80
H$^{5'}$-C5′	143.2	149.2	3.00
H$^{5''}$-C5′	143.6	157.7	7.05
Major Product Cytidine			
H$^{5'}$-C5′	149.2	174.9	12.85
H$^{5''}$-C5′	148.3	154.3	3.00
H$^{4'}$-C4′	150.0	150.9	0.45
H$^{3'}$-C3′	151.3	145.7	-2.80
H$^{2'}$-C2′	154.3	149.2	-2.55
H$^{1'}$-C1′	172.3	161.2	-5.55
H^6-C6	183.9	157.7	-13.10
H^5-C5	176.6	154.3	-11.15
Minor Product F^{5}U*			
H^6-C6	169.7	158.6	-5.55
H$^{1'}$-C1′	155.2	179.0	11.90
H$^{2'}$-C2′	159.0	157.3	-0.85
H$^{3'}$-C3′	150.4	159.0	4.30
H$^{4'}$-C4′	148.3	150.0	0.85
H$^{5'}$-C5′	144.0	151.3	3.65
H$^{5''}$-C5′	—	—	—
Minor Product Cytidine			
H$^{5'}$-C5′	151.7	175.3	11.80
H$^{5''}$-C5′	144.9	142.3	-1.30
H$^{4'}$-C4′	148.3	150.9	1.30
H$^{3'}$-C3′	148.3	146.2	-1.05
H$^{2'}$-C2′	154.3	155.6	0.65
H$^{1'}$-C1′	172.3	167.6	-2.35
H^6-C6	183.5	158.6	-12.45
H^5-C5	172.3	160.3	-6.00

An HSQC experiment with no ^{13}C-decoupling during acquisition was used to measure T_{CH} values for the major and minor products (Figures S26 and S27; Table S4). To achieve partial alignment, the products were dissolved in pentaethylene glycol monododecyl ether ($C_{12}E_5$) containing 1-hexanol.[19] This medium is widely utilized for detecting RDC values due to the ease of use and reliable formation of the lyotropic liquid crystal phase when placed in a magnetic field.[15] The D_{CH} values were then obtained through the use of Equation S2, and fit against the predicted D_{CH} values for the DFT optimized *ribo* and *arabino* 5*S*,6*R* isomers.

The RDC values derived from the major product fit the *ribo* 5*S*,6*R* product best (Q = 0.536), and the values derived from the minor product fit the *arabino* 5*S*,6*R* product best (Q = 0.619), in full agreement with the assignment. Due to the high flexibility of the phosphodiester backbone, RDC analysis of the entire dinucleotide is rendered less accurate by the averaging of the RDC values during NMR acquisition.[15] Since no rotation about the glycosidic bond is observed during DFT analysis or inferred from the HOESY data, F^{5}U* is judged to be fairly rigid. Therefore, the F^{5}U* protons should maintain a relative orientation to one another during spectral acquisition and offer a more accurate analysis of the data than treatment of the entire dinucleotide. In agreement with this premise, the fit obtained from the dinucleotides, the RDC values derived from the major product F^{5}U* fit the *ribo* 5*S*,6*R* product best (Q = 0.290), and the values derived from the minor product F^{5}U* fit the *arabino* 5*S*,6*R* product best (Q = 0.251).

DFT Chemical Shift Prediction of F^5. Fluorine chemical shifts are considered highly sensitive to the local chemical environment due to the anisotropic distribution of electrons in its 2*p* orbitals.[4,5] The chemical shifts of the minor product F^5 (−175.2 ppm) is deshielded compared to F^5 in the major product (−194.8 ppm), which suggests a significant electronic difference between the two products in the vicinity of F^5. Epimerization at C2′ moves the 2′-hydroxyl group much closer to F^5: to 2.8 Å in the *arabino* versus 4.0 Å in the *ribo* isomers. To investigate the influence of this additional hydroxyl on δ_{F5}, the iso-

Table S5. J_{HH} and J_{FH} coupling values (Hz) of the major and minor products.

nuclei	major	minor
	$F^5U^*_{(i)}$	
F^5-H^6	2.0	5.1
F^5-$H^{1'}$	26.3	34.2
$H^{1'}$-$H^{2'}$	5.5	0.7
$H^{2'}$-$H^{3'}$	5.5	4.8
$H^{3'}$-$P_{(i)}$	8.2	12.0
$H^{3'}$-$H^{4'}$	3.6	9.2
$H^{4'}$-$H^{5'}$	3.3	2.3
$H^{4'}$-$H^{5''}$	6.5	5.8
$H^{5'}$-$H^{5''}$	12.5	12.7
	$cytidine_{(i+1)}$	
$H^{5''}$-P	7.0	3.0
$H^{5'}$-P	6.0	5.0
$H^{5'}$-$H^{5''}$	12.0	11.4
$H^{4'}$-$P_{(i-1)}$	--	3.0
$H^{4'}$-$H^{5''}$	7.0	2.4
$H^{4'}$-$H^{5'}$	3.3	2.3
$H^{3'}$-$H^{4'}$	5.4	7.0
$H^{2'}$-$H^{3'}$	5.4	5.2
$H^{1'}$-$H^{2'}$	3.8	3.6
H^5-H^6	7.6	7.6
	internucleotide	
*F⁵U**F5-*Cyd*H⁵	—	1.5

tropic NMR chemical shift tensors were predicted for the converged structures of the proposed *ribo* major product and *arabino* minor product solvated in implicit water by the gauge-independent atomic orbial (GIAO) method.[20,21] In agreement with the assignment, the increased proximity of the 2′-hydroxyl reduces the shielding around F^5 in the *arabino* product (–217.6 ppm) compared to the major product (–220.7 ppm). The predicted chemical shifts are substantially more negative than the empirical values, but this trend is a known drawback of using $CFCl_3$ as a reference in ^{19}F DFT NMR calculations.[20] Even with the inherent limitations of DFT NMR prediction and the smaller difference in magnitude, the direction of chemical shift perturbation agrees with observation and supports an *arabino* minor product.

J-coupling and Pentofuranose Puckering. An interesting feature in the spectra of the minor product is the small *J*-coupling observed between $H^{1'}$ and $H^{2''}$ (0.73 Hz) and the large *J*-coupling observed between $H^{3'}$ and $H^{4'}$ (9.2 Hz) (Table S5). If the minor product is assumed for a moment to be a ribonucleoside, the equilibrium constant between interconversion of the two primary canonical puckering states, 3′-*endo* (^3E) and 2′-*endo* (^2E), can be calculated through the use of Equation S4. A value for K_{eq} of 12.6 is obtained for the minor product—almost 10-fold higher than any reported dinucleotide.[22,23]

$$K_{eq} = \frac{^3E}{^2E} = {}^3J_{H^{3'}\text{-}H^{4'}}/{}^3J_{H^{1'}\text{-}H^{2'}} \qquad \text{(S4)}$$

The rules used to derive Equation S4 can then be used to derive the relationship expressed in Equation S5, which yields the population number (p_N) as a percent of molecules in the sample residing in an ^3E pucker (^3E %), which yields an ^3E % of 93%—a value 20% larger than any reported dinucleotide.[22,23]

$$p_N \approx {}^3\text{E}\ \% \approx {}^3J_{H^{3'}\text{-}H^{4'}}/({}^3J_{H^{1'}\text{-}H^{2'}} + {}^3J_{H^{3'}\text{-}H^{4'}}) \times 100 \qquad \text{(S5)}$$

An extensive literature search failed to uncover any examples of nucelosides or dinucleotides in such a pure ^3E pucker, although dihydrouridine (D) in the trinucleotide ApDpA is in a near pure ^2E, which argues for the efficacy of the search to find examples of non-canonical bases in unusual puckers.[12,22-31] If the minor product contains a ribofuranoside and does in fact have such an extreme pucker, the equilibrium would lie strongly toward ^3E and should be apparent after DFT energy minimization. But neither the 5*S*,6*R* nor the 5*S*,6*S* isomer converges to a structure with a ^3E pucker. In fact, both products end with a ^2E pucker and never pass through ^3E during any of the optimization steps.

Since the DFT optimizations were carried out in implicit water, it is possible that an explicit water molecule or multiple water molecules would return a structure with a large degree of ^3E pucker. In a recent study, explicit water in DFT calculations resulted in structures of uridine that more accurately represent the known conformation in solution.[32] To observe the effect that explicit water molecules have on the dinucleotide products and obtain dynamic information, molecular dynamics (MD) simulations were carried out for 5 ns on the *ribo* 5*S*,6*R*, *arabino* 5*S*,6*R*, and *ribo* 5*S*,6*S* isomers in an octahedron of explicit water.

The simulation of the *ribo* 5*S*,6*R* isomer resulted in a distribution of 60% ^3E (Figure S28, panel A), whereas analysis of the *J*-coupling values (Table S5) suggests 40% ^3E. These values agree reasonably well and lie on opposite ends of the range observed for canonical dinucleotides in solution.[22,23] The *J*-couplings in the minor product suggest 93% ^3E in disagreement with the MD simulations, which suggest 6.7% ^3E for the 5*S*,6*S* isomer (Figure S28, panel B) and a pucker between the canonical *arabino* pucker of O4′-*endo* (^OE) and ^2E for the *arabino* minor product (Figure S28, panel C). The *J* values, then, predict an ^3E pucker in the minor product that the MD simulations may underrepresent.

A possible explanation for the MD simulation not accurately modeling the *arabino* product is the abnormality of the F^5U^* and inaccurate modeling of fluorine. With careful shimming (DSS line width at half height of <0.50 Hz), a *J*-coupling (1.46 Hz) was revealed between H^5 of cytidine and F^5 in the minor product (Figure S29). Because the skeletal structures of the major and minor product are identical (and the number of intervening bonds is tremendous), the small coupling must arise from spatial orientation. The transmission of scalar coupling through hydrogen bonds has been know for almost two decades[33], and a literature search confirmed that J_{HF} scalar coupling through hydrogen bonds have been observed between aromatic protons and sp^3 fluorine atoms in nucleosides, although not in aqueous solution.[34,35] Analysis of the HOESY spectrum confirms that F^5 is correlated with cytidine H^5, and in fact, integrates larger than $H^{1'}$ of F^5U^*. This result suggests that for a period of time, H^5 of cytidine resides close enough to F^5 for scalar coupling to develop, either directly or through a water molecule. This interaction could draw F^5 closer to C2′ and move the population distribution of the *arabino* product towards the ^2E pucker in solution.

In addition to the $\phi_{H^{1'}\text{-}H^{2''}}$ of a ^2E pucker causing a reduction in the observed $^3J_{H^{1'}\text{-}H^{2''}}$, the magnitudes of *J*-couplings are also influenced by substituent electronegativity, bond angle, and bond length.[36-38] With such an unusual *C*-glycosidic linkage in which both carbon atoms are saturated and one has a fluoro group, and with $H^{1'}$ *trans* to the 2′-hydroxyl and F^5, the generalized relationship between coupling values and pentofuranose pucker may not strictly apply.[39] The unusual glycosidic linkage may influence bond angles between $H^{1'}$ and $H^{2''}$ Altering bond angles by as little as 5° has been shown to have large influences on *J*-couplings, especially in fluorinated compounds.[3,5,38,40] Also, the similar van der Waals radii of oxygen and fluorine may lead to a significant steric clash with the 2′-OH in the arabinofuranose, causing strain but simultaneously allowing a possible new hydrogen bond between them. All of these factors could contribute to contort the $H^{2'}$-C2′-C1′ and $H^{1'}$-C1′-C2′ bond angles, stretch the C2′-C1′ bond, or both, thus reducing electron overlap and altering $J_{H^{1'}\text{-}H^{2'}}$ in unexpected ways.

However, the most likely cause for the discrepancy between the pucker of the minor product predicted by MD simulations and the pucker predicted by *J* coupling analysis is the derivation of the latter from data accumulated with ribofuranosides. The inadequacy of

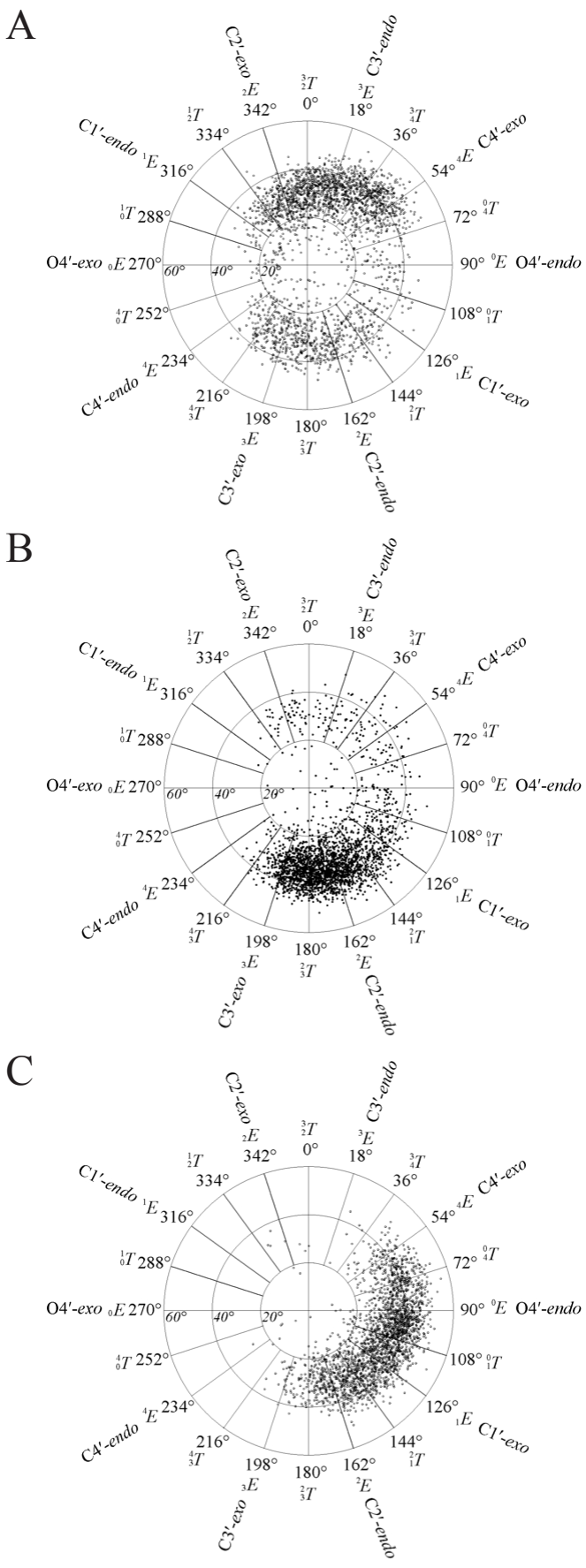

Figure S28. The pseudorotational phase and amplitude plot[45] of the MD simulation with (A) the proposed (5*S*,6*R*) major product; (B) the discounted 5*S*,6*S* isomer; (C) the *arabino* minor product.

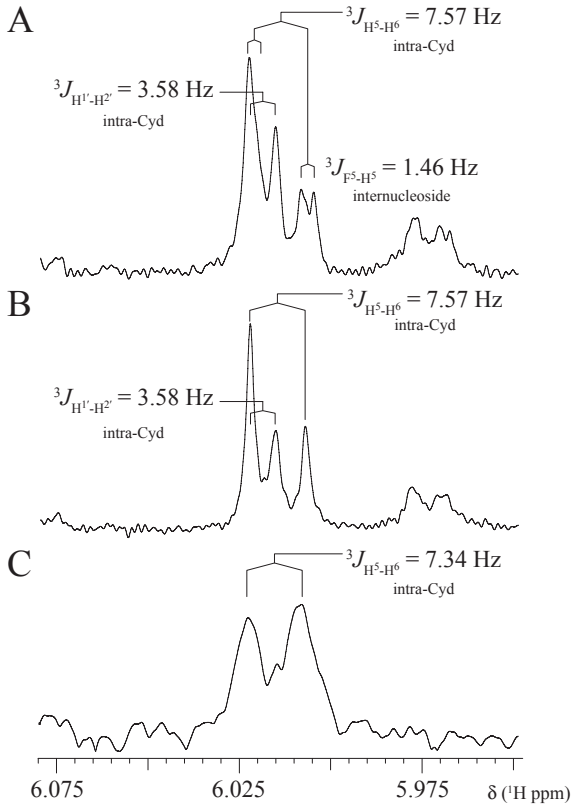

Figure S29. Long-range *J* coupling between H^5 of cytidine and F^5 of F^5U* in the minor product. (A) The fully coupled ^{1}H spectrum. (B) The {^{19}F} ^{1}H spectrum. (C) The 1D ^{1}H-^{19}F HSQC spectrum. All couplings are within the cytidine moiety ("intra-Cyd") except for H^5-F^5 ("internucleoside").

this standard pucker assignment from *J*-coupling analysis for α-arabinofuranosides has been reported[41] and even greater difficulties with β-arabinofuranosides (such as the proposed minor product) have been very recently noted.[42]

Experimental

NMR. NMR spectra were acquired using a DRX 400 spectrometer equipped with a 5 mm QNP probe (Bruker BioSpin Corp., Billerica, MA), an AVANCE 600 spectrometer equipped with a 5mm HCN z-PFG CryoProbe (Bruker), a Varian 400-MR spectrometer equipped with a 5 mm direct HX z-PFG broadband probe (Varian Inc., Palo Alto, CA), an INOVA 500 spectrometer equipped with a 5 mm inverse HFX z-PFG probe (Wang NMR, Inc., Livermore, CA) or a 5 mm direct HX broadband probe (Varian), a VNMRS 700 spectrometer equipped with a 5 mm inverse HCN z-PFG cryogenic probe (Varian), or a VNMRS 800 spectrometer equipped with a 5 mm inverse HCN z-PFG probe (Varian). Minimal changes to the *ghsqc_d2* pulse sequence (Varian) were required to detect ^{1}H-^{19}F correlation. All other pulse sequences were used as provided and configured as suggested by the manufacturer. Spectra were processed with VNMRJ v2.1c (Varian), TopSpin v2.x (Bruker), MestReC v4.9.9.6 (Mestrelab Research, Santiago de Compostela, Spain) and MestReNova v6.0.2-5475 (Mestrelab Research).

Product generation and NMR assignment. The large scale formation and isolation of the products of F^5U from the action of TruB has been described in detail for the samples used in the experiments reported here.[43] The major and minor product samples were originally isolated as a mixture. The presented values come largely from the last samples in which the two products were largely separated, but no change in chemical shift was noted in the different samples. The measured *J*-couplings were checked through the use of spin simulation software (MestReC v4.9.9.6, MestReLab Research).

Major dinucleotide product, cis-(5S,6R)-6-hydroxy-5-fluoropseudouridylyl-(5′→3′)-cytidine. F^5U^*, *cis*-(5*S*,6*R*)-6-hydroxy-5-fluoropseudouridine: ^{1}H NMR (700 MHz, D_2O) δ 5.340 (1H, d, $^3J_{F5}$ = 2.0 Hz, H^6), 4.449 (1H, dd, $^3J_{H1'}$ = 5.5, $^3J_{H3'}$ 5.5 Hz, H$^{2'}$), 4.413 (1H, ddd, ^3J_P = 8.2, $^3J_{H2'}$ = 5.5, $^3J_{H4'}$ = 3.6 Hz, H$^{3'}$), 4.264 (1H, dd, $^3J_{F5}$ = 26.3, $^3J_{H2'}$ = 5.5 Hz, H$^{1'}$), 4.194 (1H, ddd, $^3J_{H5''}$ = 6.5, $^3J_{H3'}$ = 3.6, $^3J_{H5'}$ = 3.3 Hz, H$^{4'}$), 3.774 (1H, dd, $^2J_{H5''}$ = 12.5, $^3J_{H4'}$ = 3.3 Hz, H$^{5'}$), 3.609 (1H, dd, $^2J_{H5'}$ = 12.5, $^3J_{H4'}$ = 6.5 Hz, H$^{5''}$); ^{13}C NMR (700 MHz, gHSQC/gHMBC, D_2O) δ 170.4 (C4), 156.2 (C2), 93.7 (C5, d, $^1J_{CF}$ = 192.5 Hz), 86.2 (C4′, d, $^1J_{CH}$ = 151.3 Hz), 83.6 (C1′, d, $^1J_{CH}$ = 150.9 Hz), 77.6 (C3′, d, $^1J_{CH}$ = 156.4 Hz), 75.7 (C6, d, $^1J_{CH}$ = 169.7 Hz), 72.0 (C2′, d, $^1J_{CH}$ = 152.6 Hz), 63.9 (C5′, dd, $^1J_{CH}$ = 143.6, 143.2 Hz); ^{19}F NMR (470 MHz, D_2O) δ −194.8 (F^5, d, $^3J_{H1'}$ = 26.3 Hz); ^{31}P (202 MHz, D_2O) δ −1.577 (P_{i+1}). Cytidine: ^{1}H NMR (700 MHz, D_2O) δ 7.908 (1H, d, $^3J_{H5}$ = 7.6 Hz, H^6), 6.083 (1H, d, ^3J_H6 = 7.6 Hz, H^5), 5.972 (1H, d, $^3J_{H2'}$ = 3.8 Hz, H$^{1'}$), 4.307 (1H, dd, $^3J_{H2'}$ = 5.4, $^3J_{H4'}$ = 5.4 Hz, H$^{3'}$), 4.291 (1H, dd, $^3J_{H3'}$ = 5.4, $^3J_{H1'}$ = 3.8 Hz, H$^{2'}$), 4.247 (1H, ddd, $^2J_{H5''}$ = 12.0, $^3J_{H4'}$ = 3.3, ^3J_P = 6.0 Hz, H$^{5''}$), 4.238 (1H, ddd, $^3J_{H5''}$ = 7.0, $^3J_{H3'}$ = 5.4, $^3J_{H5'}$ = 3.3 Hz, H$^{4'}$), 4.115 (1H, ddd, $^2J_{H5'}$ = 12.0, ^3J_P = 7.0, $^3J_{H4'}$ = 7.0 Hz, H$^{5''}$); ^{13}C NMR (700 MHz, gHSQC/gHMBC, D_2O) δ 168.8 (C4), 160.3 (C2), 143.9 (C6, d, $^1J_{CH}$ = 183.9 Hz), 99.0 (C5, d, $^1J_{CH}$ = 176.6 Hz), 92.2 (C1′, d, $^1J_{CH}$ = 172.3 Hz), 84.9 (C4′, d, $^1J_{CH}$ = 150.0 Hz), 76.7 (C2′, d, $^1J_{CH}$ = 154.3 Hz), 71.7 (C3′, d, $^1J_{CH}$ = 151.3 Hz), 66.8 (C5′, d, $^1J_{CH}$ = 149.2, 148.3 Hz).

Minor dinucleotide product, cis-(5S,6R)-6-hydroxy-5-fluoropseudouridine-β-1-D-arabinofuranosylyl-(5′→3′)-cytidine. F^5U^*, *cis*-(5*S*,6*R*)-6-hydroxy-5-fluoropseudourine-β-1-D-arabinofuranoside: ^{1}H NMR (700 MHz, D_2O) δ 5.206 (1H, d, $^3J_{F5}$ = 5.1 Hz, H^6), 4.649 (1H, d, $^3J_{H3'}$ = 4.8 Hz, H$^{2''}$), 4.377 (1H, dd, $^3J_{F5}$ = 34.2, $^3J_{H2''}$ = 0.7 Hz, H$^{1'}$), 4.278 (1H, ddd, ^3J_P = 12.0, $^3J_{H4'}$ = 9.2, $^3J_{H2''}$ = 4.8 Hz, H$^{3'}$), 4.051 (1H, ddd, $^3J_{H2'}$ = 9.2, $^3J_{H5''}$ = 5.8, $^3J_{H5'}$ = 2.3 Hz, H$^{4'}$), 3.926 (1H, dd, $^2J_{H5''}$ = 12.7, $^3J_{H4'}$ = 2.3 Hz, H$^{5'}$), 3.661 (1H, dd, $^2J_{H5'}$ = 12.7, $^3J_{H4'}$ = 5.8 Hz, H$^{5''}$); ^{13}C NMR (700 MHz, gHSQC/gHMBC, D_2O) δ 168.4 (C4), 155.7 (C2), 90.7 (C5, d, $^1J_{CF}$ = 200.7 Hz), 85.6 (C1′, d, $^1J_{CH}$ = 155.2 Hz), 82.4 (C4′, d, $^1J_{CH}$ = 148.3 Hz), 76.5 (C3′, d, $^1J_{CH}$ = 150.4 Hz), 75.4 (C6, d, $^1J_{CH}$ = 169.7 Hz), 74.2 (C2′, d, $^1J_{CH}$ = 159.0 Hz), 63.6 (C5′, d, $^1J_{CH}$ = 144.0 Hz); ^{19}F NMR (470 MHz, D_2O) δ −175.2 (F^5, d, $^3J_{H1'}$ = 34.2 Hz); ^{31}P (202 MHz, D_2O) δ −1.811 (P_{i+1}). Cytidine: ^{1}H NMR (700 MHz, D_2O) δ 7.867 (H^6, d, $^3J_{H5}$ = 7.6 Hz), 6.022 (1H, d, $^3J_{H2'}$ = 3.6 Hz, H$^{1'}$), 6.015 (1H, dd, $^3J_{H6}$ = 7.6, J_{F5} = 1.5 Hz, H^5), 4.362 (1H, dd, $^3J_{H4'}$ = 7.0, $^3J_{H2'}$ = 5.2 Hz, H$^{3'}$), 4.354 (1H, ddd, $^2J_{H5''}$ = 11.4, ^3J_P = 5.0, $^3J_{H4'}$ = 2.3 Hz, H$^{5'}$), 4.242 (1H, dd, $^3J_{H3'}$ = 5.2, $^3J_{H1'}$ = 3.6 Hz, H$^{2'}$), 4.208 (1H, ddd, $^3J_{H3'}$ = 7.0, ^4J_P = 3.0, $^3J_{H5''}$ = 2.4, $^3J_{H5'}$ = 2.3 Hz, H$^{4'}$), 4.086 (1H, ddd, $^2J_{H5'}$ = 11.4, ^3J_P = 3.0, $^3J_{H4'}$ = 2.4 Hz, H$^{5''}$); ^{13}C NMR (700 MHz, gHSQC/gHMBC, D_2O) δ 168.3 (C4), 160.1 (C2), 143.5 (C6, d, $^1J_{CH}$ = 183.5 Hz), 99.4 (C5, d, $^1J_{CH}$ = 172.3 Hz), 92.2 (C1′, d, $^1J_{CH}$ = 172.3 Hz), 84.3 (C4′, d, $^1J_{CH}$ = 148.3 Hz), 76.9 (C2′, d, $^1J_{CH}$ = 154.3 Hz), 71.3 (C3′, d, $^1J_{CH}$ = 148.3 Hz), 66.2 (C5′, d, $^1J_{CH}$ = 151.7, 144.9 Hz).

Chemical Degradation with Periodiate. Isolated dinucleotide products (0.6 μmol) were dissolved in 500 mM ammonium bicarbonate buffer (1.2 mL), pH 8, and sodium metaperiodate (6 μmol) was added. The mixture was incubated for 90 min at 60 °C in a blacked-out microcentrifuge tube to prevent destruction of the periodate by UV light. After 90 min, the reaction mixture was taken to dryness *in vacuo* and redissolved in water (400 μL). After four such cycles, nearly all ammonium bicarbonate was judged to be removed by the lack of effervescence upon redissolution of the residue. Excess sodium metaperiodate was destroyed by the addition of glycerol (30 μmol) and incubation for 5 min at 22 °C, after which the reaction mixture was adjusted to pH 1.9 by the addition of hydrochloric acid (1.3 μL; 6 M). After 30 min at 60 °C, the reaction was neutralized with ammonia water (1.4 μL; 7.4 M) and taken to dryness *in vacuo*. The products were dissolved in D_2O and NMR spectra acquired.

The nucleotide 3′-monophosphate products were purified by weak anion exchange chromatography. A small column (500 μL) of Capto DEAE (90 μm; GE Healthcare, Chalfont St. Giles, UK) was poured in a disposable Pasteur pipette (5¾ in × 4 mm ID) plugged with glass wool. The column was prepared by washing with 250 mM ammonium bicarbonate buffer (5 mL), pH 8, and then pre-equilibrated with 20 mM ammonium bicarbonate buffer (5 mL), pH 8, at which point the pH and conductivity of the column eluate matched that of the 20 mM ammonium bicarbonate buffer. The nucleotide 3′-monophosphate products were diluted with 10 mM ammonium bicarbonate buffer (to 5 mL final volume), pH 8, and after ensuring that the conductivity of the sample was less than that of the buffer in which the column was pre-equilibrated, the sample was loaded on the Capto DEAE column. The nucleotide 3′-monophosphate products were eluted using a 5-step gradient (2.5 mL each step), with each step increasing 10 mM in buffer concentration.

The fractions were dried *in vacuo*, redissolved in D_2O, and analyzed by NMR to locate the products, the bulk of which eluted at 60 mM buffer with trace amounts at 50 mM. The eluates of these two gradient steps were combined, taken to dryness *in vacuo*, and redissolved in water. After four such cycles, nearly all ammonium bicarbonate was judged to be removed by the lack of effervescence upon redissolution of the residue. The final sample was redissolved in 10 mM sodium phosphate buffer in D_2O (300 μL), pD 7.9, containing sodium 4,4-dimethyl-4-silapentane-1-sulfonate-d_6 (0.12 mM; kindly provided by T. Fan, U. of Louisville), and subjected to NMR analysis.

^{1}H NMR (700 MHz, D_2O) δ 5.347 (1H, d, $^3J_{F5}$ = 1.9 Hz, H^6), 4.423 (1H, dd, $^3J_{H1'}$ = 5.2, $^3J_{H3'}$ = 5.2 Hz, H$^{2'}$), 4.318 (1H, ddd, ^3J_P = 8.2, $^3J_{H4'}$ = 6.0, $^3J_{H2'}$ = 5.2 Hz, H$^{3'}$), 4.253 (1H, dd, $^3J_{F5}$ = 26.3, $^3J_{H2'}$ = 5.2 Hz, H$^{1'}$), 4.110 (1H, ddd, ^3J_H5″ = 6.6, ^3J_H3′ = 6.0, ^3J_H5′ = 3.5 Hz, H$^{4'}$), 3.797 (1H, dd, ^2J_H5″ = 12.4, ^3J_H4′ = 3.5 Hz, H$^{5'}$), 3.642 (1H, dd, $^2J_{H5'}$ = 12.5, $^3J_{H4'}$ = 6.6 Hz, H$^{5''}$); ^{13}C NMR (700 MHz, gHSQC/gHMBC, D_2O) δ 171.1 (C4), 156.7 (C2), 93.7 (C5), 86.1 (C4′, d, $^1J_{CH}$ = 153.6 Hz), 84.3 (C1′, d, $^1J_{CH}$ = 151.2 Hz), 76.4 (C3′, d, $^1J_{CH}$ = 153.4 Hz), 75.6 (C6, d, $^1J_{CH}$ = 168.3 Hz), 72.6 (C2′, d, $^1J_{CH}$ = 151.8 Hz), 64.3 (C5′, dd, $^1J_{CH}$ = 143.3, 142.1 Hz); ^{19}F NMR (470 MHz, D_2O) δ −193.3 (F^5, d, $^3J_{H1'}$ = 27.1 Hz); ^{31}P (202 MHz, D_2O) δ 1.245 (P$^{3'}$)

Residual Dipolar Couplings. The separated TruB products were dried *in vacuo* and dissolved in D_2O (200 μL), after which $C_{12}E_5$ was added (490 μL) to a final concentration of 7% and homogenized by vortex mixing. Neat 1-hexanol (7.96 M) was added step wise (1 μL/step) followed by vortex mixed after each step until the desired molar ratio was achieved (r = 0.90). The opalescent sample was transferred to an NMR tube, placed in the magnet, and equilibrated for 2 h at 30 °C. Once ^{2}H splitting was stable (~45 Hz), the probe temperature was reduced to 25 °C and the sample was allowed to equilibrate for an additional 2 h.[19] To detect *T*-coupling, a phase sensitive, gradient enhanced ^{1}H–^{13}C DEPT-HSQC spectrum was acquired with presaturation centered on the methylene peak of $C_{12}E_5$. The detected RDC values were fit against the DFT optimized structures utilizing the singular value decomposition (SVD) method with an error of 0.5 Hz and a Gaussian distribution of 128 (MSpin v1.2.1-49; MestReLab Research S.L., Santiago de Compostela, Spain).

Formation and Isolation of Ψ and the F^5U Products after Incubation of RNA with TruB in Buffered D_2O. Deuterated reaction buffer was prepared from unlabled reaction buffer, which is 50 mM HEPES, pH 7.5, containing ammonium chloride (100 mM), dithiothreitol (5 mM), and EDTA (1 mM). Unlabeled reaction buffer was lyophilized to dryness and redissolved in D_2O (>99%) three times. TruB (10 μM) and TSL (100 mM) were exchanged into deuterated reaction buffer (20 μL) prior to their incubation together for 10 min at 37 °C. The modified RNA was digested and isolated as described above. Briefly, S1 nuclease and alkaline phosphatase were added to the mixture, and after digestion, Ψ was isolated by isocratic reverse-phase HPLC. The

fractions containing Ψ were dried *in vacuo*, re-dissolved in water, and an aliquot (0.25 μL) was subjected to high resolution mass spectrometric analysis by dissolution into aqueous methanol (50%). No peaks were detected for a species in which a proton at C2′ was replaced with a deuteron. The F^5U products were produced identically (except that the reaction volume was doubled), then isolated, and subjected to mass spectrometric analysis. No mass peaks containing the replacement of a proton with a deuteron at C2′ were detected.

Density Functional Theory Calculations. The starting structure for *cis*-(5*S*,6*R*)-6-hydroxy-5-fluoropseudouridylyl-(5′→3′)-cytidine was obtained from the cocrystal of TruB and [F^5U]TSL (PDB entry 1K8W). The dinucleotide was opened in Chem3D (v8.0; CambridgeSoft Corp., Cambridge, MA), protonated, and after manual inversion (at C5, C6 and C2′) each stereochemical isomer was saved separately as Cartesian coordinates and edited to include proper headers for Gaussian 09 (Gaussian Inc, Wallington, CT) DFT optimization:

```
%chk=name.chk
%nproc=8
%mem=2GB
#P B3LYP/6-311+G(2d,p) Opt SCRF=(CPCM)

name

-1  1
XYZ Coordinates
(Return)
(Return)
```

All stereoisomers were minimized with Gaussian 09 IBM64-G09RevA.02 on IBM PowerPC 4.7 GHz processors running AIX 6.1.

To calculate NMR shielding tensors, the converged structures were submitted to Gaussian 09 with the following headers:

```
%chk=name.chk
%nproc=8
%mem=2GB
#P mPW1PW91/6-311+G(2d,p) NMR SCRF=(CPCM)

name

-1 1
XYZ Coordinates
(Return)
(Return)
```

Molecular Dynamics Simulations. The molecular dynamic simulations on the dinucleotide product isomers required modified AMBER force field parameters.[44] The converged DFT structures were prepared for RESP charge fitting by carrying out the electrostatic potential (ESP) calculation with Gaussian 09 using the following headers:

```
%chk=name.chk
%nproc=8
%mem=1GB
#P HF/6-31G(d) SCF=Tight Test Pop=MK iop(6/33=2) iop(6/42=6)

name

-1  1
XYZ Coordinates
(Return)
(Return)
```

To obtain frcmod and prepc files, RESP charge fitting was carried out using the *antechamber*, *atomtype*, *prepgen*, and *parmchk* modules of AMBER 10 (University of California, San Francisco) and the output file *name*.log obtained from the Gaussian 09 ESP charge calculation. The following commands were performed sequentially:

```
antechamber -fi gout -fo prepi -i name.log -o name.prepi -c   //
resp -j both -at amber -rn name

antechamber -fi gout -fo ac -i name.log -o name_resp.ac -c resp

antechamber -fi ac -i name_resp.ac -c wc -cf name.crg

atomtype -i name_resp.ac -o name_resp_gaff.ac -p gaff

prepgen -i name_resp_gaff.ac -o name_resp_gaff.prepc -f car

parmchk -i name_resp_gaff.prepc -o name.frcmod -f prepc
```

To obtain the solvated topology and coordinate files, the frcmod and prepc files were loaded into *tleap* (part of the AMBER 10 suite) and solvated in an octahedron of TIP3PBOX water.

The topology and coordinate files were then prepared for full MD simulation by first minimizing the solvent while keeping the solute fixed, then minimizing the entire system, and finally heating the entire system from 0 K to 300 K. Due to limitations imposed by the computer node scheduler, the full simulations were only able to run for 24 h, which ended each simulation after 5.8 to 6.0 ns. In the interest of consistency, each isomer was therefore only analyzed from 0.5 ns to 5.5 ns for an effective simulation run time of 5 ns. Each input file is listed below. All AMBER10 programs except *sander* were executed on one Intel Xeon L5420 2.5GHz processor running Red Hat Linux 5.2 with kernel 2.6.18-92.el5-x86_64; *sander* was run on eight Intel Xeon L5420 2.5GHz processors using *sander.MPI*, which was compiled to use openmpi running on Red Hat Linux 5.2 with kernel 2.6.18-92.el5-x86_64. Output coordinate files were analyzed with VMD (v1.8.7; University of Illinois, Urbana-Champaign).

```
initial minimisation solvent
    &cntrl
     imin   = 1,
     maxcyc = 1000,
     ncyc   = 500,
     ntb    = 1,
     ntr    = 1,
     cut    = 10
    /
   Hold the dinucleotide fixed
   500.0
   RES 1
   END
   END

initial minimisation whole system
    &cntrl
     imin   = 1,
     maxcyc = 2500,
     ncyc   = 1000,
     ntb    = 1,
     ntr    = 0,
     cut    = 10
    /

20ps MD with res on dinucleotide
    &cntrl
     imin   = 0,
     irest  = 0,
     ntx    = 1,
     ntb    = 1,
     cut    = 10,
     ntr    = 1,
     ntc    = 2,
     ntf    = 2,
     tempi  = 0.0,
     temp0  = 300.0,
     ntt    = 3,
     gamma_ln = 1.0,
     nstlim = 10000, dt = 0.002
     ntpr = 100, ntwx = 100, ntwr = 1000
    /
   Keep dinucleotide fixed with weak restraints
   10.0
   RES 1
   END
   END

6 ns MD
    &cntrl
     imin = 0, irest = 1, ntx = 7,
     ntb = 2, pres0 = 1.0, ntp = 1,
     taup = 2.0,
     cut = 10, ntr = 0,
     ntc = 2, ntf = 2,
     tempi = 300.0, temp0 = 300.0,
     ntt = 3, gamma_ln = 1.0,
     nstlim = 3000000, dt = 0.002,
     ntpr = 100, ntwx = 100, ntwr = 1000
    /
```

REFERENCES

References are numbered independently of the main text.

(1) Claridge, T. D. W. *High-Resolution NMR Techniques in Organic Chemistry*; Elsevier, 1999; Vol. 19.
(2) Jacobsen, N. E. *NMR Spectroscopy Explained: Simplified Theory, Applications and Examples for Organic Chemistry and Structural Biology*; John Wiley & Sons, Inc.: Hoboken, NJ, 2007.
(3) Williamson, K. L.; Hsu, Y.-F. L.; Hall, F. H.; Swager, S.; Coulter, M. S. *J. Am. Chem. Soc.* **1968**, *90*, 6717.
(4) Hennig, M.; Munzarová, M. L.; Bermel, W.; Scott, L. G.; Sklenář, V.; Williamson, J. R. *J. Am. Chem. Soc.* **2006**, *128*, 5851.
(5) Cushley, R. J.; Wempen, I.; Fox, J. J. *J. Am. Chem. Soc.* **1968**, *90*, 709.
(6) Roberts, L.-Y. L. a. G. C. K. *NMR of Macromolecues: A Practical Approach*; Oxford University Press: New York, 1993.
(7) Ermolinsky, B.; Mikhailov, S. *Russ. J. Bioorg. Chem*. **2000**, *26*, 429.
(8) Khym, J. X.; Cohn, W. E. *J. Biol. Chem.* **1961**, *236*, PC9.
(9) Spedaliere, C. J.; Mueller, E. G. *RNA* **2004**, *10*, 192.
(10) Hoang, C.; Ferré-D'Amaré, A. R. *Cell* **2001**, *107*, 929.
(11) Remin, M.; Darzynkiewicz, E.; Dworak, A.; Shugar, D. *J. Am. Chem. Soc.* **1976**, *98*, 367.
(12) Ancian, B. *Annu. Rep. NMR Spectrosc.* **2010**, *69*, 39.
(13) Gschwind, R. M. *ChemInform* **2005**, *36*, 4666.
(14) Kummerlöwe, G.; Luy, B. *TrAC, Trends Anal. Chem.* **2009**, 28, 483.
(15) Thiele, C. M. *Eur. J. Org. Chem.* **2008**, *2008*, 5673.
(16) Duer, M. J. In *Solid-State NMR Spectroscropy Principles and Applications*; Duer, M. J., Ed.; Wiley-Blackwell: 2007.
(17) Kramer, F.; Deshmukh, M. V.; Kessler, H.; Glaser, S. J. *Concepts Magn. Reson. Part A* **2004**, *21A*, 10.
(18) Cornilescu, G.; Marquardt, J. L.; Ottiger, M.; Bax, A. *J. Am. Chem. Soc.* **1998**, *120*, 6836.
(19) Rückert, M.; Otting, G. *J. Am. Chem. Soc*. **2000**, *122*, 7793.
(20) Williams, D. E.; Peters, M. B.; Wang, B.; Merz, K. M. *J. Phys. Chem. A* **2008**, *112*, 8829.
(21) Fukaya, H.; Ono, T. *J. Comput. Chem.* **2004**, *25*, 51.
(22) Lee, C.-H.; Ezra, F. S.; Kondo, N. S.; Sarma, R. H.; Danyluk, S. S. *Biochemistry* **1976**, *15*, 3627.
(23) Tran-Dinh, S.; Neumann, J. M.; Borrel, J. *Biochim. Biophys. Acta, Nucl. Acids Prot. Synth.* **1981**, *655*, 167.
(24) Day, R. O.; Seeman, N. C.; Rosenberg, J. M.; Rich, A. *Proc. Natl. Acad. Sci. U.S.A.* **1973**, *70*, 849.
(25) Johnson, N. P.; Switkes, E.; Schleich, T. *J. Am. Chem. Soc.* **1976**, *98*, 7535.
(26) Loomis, R. E.; Alderfer, J. L. *Biopolymers* **1986**, *25*, 571.
(27) Parthasarathy, R.; Malik, M.; Fridey, S. M. *Proc. Natl. Acad. Sci. U.S.A.* **1982**, *79*, 7292.
(28) Seeman, N. C., Sussman, J. L., Berman, H. M., S. H. Kim *Nature New Biology* **1971**, *233*, 90.
(29) Uesugi, S.; Kaneyasu, T.; Imura, J.; Ikehara, M.; Cheng, D. M.; Kan, L.; Ts'o, P. O. P. *Biopolymers* **1983**, *22*, 1189.
(30) Dalluge, J. J.; Hashizume, T.; Sopchik, A. E.; McCloskey, J. A.; Davis, D. R. *Nucleic Acids Res*. **1996**, *24*, 1073.
(31) Chang, Y.-C.; Herath, J.; Wang, T. H. H.; Chow, C. S. *Bioorg. Med. Chem.* **2008**, *16*, 2676.
(32) Barbe, S.; Le Bret, M. *J. Phys. Chem. A* **2008**, *112*, 989.
(33) Blake, P.; Lee, B.; Summers, M.; Adams, M.; Park, J.-B.; Zhou, Z.; Bax, A. *J. Biomol. NMR* **1992**, *2*, 527.
(34) Mele, A.; Vergani, B.; Viani, F.; Meille, S. V.; Farina, A.; Bravo, P. *Eur. J. Org. Chem*. **1999**, *1999*, 187.
(35) Bartolomé, C.; Espinet, P.; Martín-Alvarez, J. M. *Chem. Commun.* **2007**, 4384.
(36) Haasnoot, C. A. G.; de Leeuw, F. A. A. M.; Altona, C. *Tetrahedron* **1980**, *36*, 2783.
(37) Thibaudeau, C.; Plavec, J.; Chattopadhyaya, J. *J. Org. Chem.* **1998**, *63*, 4967.
(38) Barfield, M.; Smith, W. B. *J. Am. Chem. Soc.* **1992**, *114*, 1574.
(39) Jaworski, A.; Ekiel, I.; Shugar, D. *J. Am. Chem. Soc.* **1978**, *100*, 4357.
(40) Hall, L. D.; Jones, D. L. *Can. J. Chem.* **1973**, *51*, 2925.
(41) Taha, H. A.; Castillo, N.; Sears, D. N.; Wasylishen, R. E.; Lowary, T. L.; Roy, P.-N. *J. Chem. Theory Comput.* **2009**, *6*, 212.
(42) Taha, H. A.; Roy, P.-N.; Lowary, T. L. *J. Chem. Theory Comput.* **2011**, DOI: 10.1021/ct100450s.
(43) McDonald, M. K.; Miracco, E. J.; Chen, J.; Xie, Y.; Mueller, E. G. *Biochemistry* **2011**, *50*, 426.
(44) Aduri, R.; Psciuk, B. T.; Saro, P.; Taniga, H.; Schlegel, H. B.; SantaLucia, J. *J. Chem. Theory Comput.* **2007**, *3*, 1464.
(45) Markley, J. L.; Bax, A.; Arata, Y.; Hilbers, C. W.; Kaptein, R.; Sykes, B. D.; Wright, P. E.; Wüthrich, K. *J. Mol. Biol.* **1998**, *280*, 933.